[American Journal of Science, Vol. 320, May, 2020, P. 405–449, DOI 10.2475/05.2020.01]

American Journal of Science

MAY 2020

AVALONIAN ARC-TO-PLATFORM TRANSITION IN SOUTHEASTERN NEW ENGLAND: U-Pb GEOCHRONOLOGY AND STRATIGRAPHY OF EDIACARAN CAMBRIDGE "ARGILLITE," BOSTON BASIN, MASSACHUSETTS, USA

MARGARET D. THOMPSON*,† and JAMES L. CROWLEY**

ABSTRACT. High-precision CA-TIMS $^{206}Pb/^{238}U$ zircon dates clarify the age and tectonic significance of the Cambridge Formation which is poorly exposed in the Boston Basin, eastern Massachusetts, but transected by ~50 km of tunnels beneath the mainland and Boston Harbor. The youngest detrital zircon in a sample from the northern Braintree Weymouth Tunnel establishes a maximum depositional age of 584.09 ± 1.98 Ma, consistent with sources in sills of that age in underlying Roxbury Conglomerate. A 551.22 ± 0.20 Ma ash bed from the Mystic Quarry in Somerville, Massachusetts lies near the top of an approximately 5350 m thick, dominantly argillaceous section measured in subsurface cross sections.

These were constructed from attitudes reported in pre-1960 tunnels and from mapping logs obtained from tunnels completed decades later during the federally ordered clean-up of Boston Harbor. A 488.58 ± 0.16 Ma aplite sill intruding argillite ~800 m above the ash bed sets the minimum depositional age on the north side of the Basin. A tighter constraint comes from trilobite-bearing strata of the lower Cambrian Weymouth Formation located south of Boston that overlies the Cambridge Formation without obvious break in the Braintree Weymouth Tunnel. If Cambridge deposition was continuous after 584 Ma, the depositional interval would exceed 40 million years. An estimated ~20 Ma depositional hiatus seems more likely because the base of the Cambridge Formation appears to define a regional unconformity above which argillite rests variously on magmatic arc-related units of both the 595 to 584 Ma Roxbury Conglomerate and the 597 to 593 Ma Lynn-Mattapan Volcanic Complex.

Cambridge deposition set in once arc activity in more northerly "West" Avalonian terranes extending through Atlantic Canada to the Avalon Peninsula, Newfoundland had given way to wrench faulting and bimodal magmatism. This regime is manifested structurally in Boston-area tunnels by later-reactivated normal faults in which hanging wall blocks of Cambridge argillite were originally downthrown relative to older footwall units. Pyroclastic volcanic textures and thin basaltic flows with soft sediment contacts are present in argillite of the City Tunnel Extension, and whole rock major element and REE compositions reveal mixed terrigenous and volcanic components deposited under marine conditions throughout the Basin. Proposed sources for the latter are voluminous eruptions recorded in the 560 to 550 Ma Coldbrook Group in New Brunswick's Caledonia terrane.

Keywords: Cambridge Formation, Boston Basin, tunnels, U-Pb geochronology, Avalonian tectonics

* Department of Geosciences, Wellesley College, Wellesley, Massachusetts 02481
** Department of Geosciences, Boise State University, Boise, Idaho 83725-1535
† Corresponding author: mthompson@wellesley.edu

INTRODUCTION

Fossiliferous Cambrian shales resting locally on widespread granitoid basement of presumed Precambrian age (Billings, 1929; Dowse, 1950) prompted early interpretations linking SE New England east of the Lake Char and Bloody Bluff faults with the Avalon Peninsula of Newfoundland (fig. 1; Rodgers, 1967 and 1972; Rast and others, 1976; Williams, 1978; Skehan and others, 1978). Pioneering U-Pb zircon geochronology shortly thereafter confirmed the Proterozoic Z origin of granites and volcanic rocks in the vicinity of Boston, Massachusetts (upper concordia intercept dates from batch zircon analyses of Kaye and Zartman, 1980; Zartman and Naylor, 1984; Ediacaran in current timescales). These results together with more abundant dates from Canadian localities gave rise to more detailed tectonostratigraphic analysis in a succession of papers starting with Murphy and Nance (1989) and elaborated as additional information emerged (Nance and Murphy, 1996: Murphy and others, 2000; Nance and others, 2002, 2008). According to this model, northern Appalachian "West" Avalonian terranes (inset map in fig. 1) experienced early subduction (~730–650 Ma) in arcs developed on ~1.3 to 1.0 Ga juvenile crust in the ocean surrounding Rodinia. The early arcs were accreted to the Gondwanan margin, and after a lull, subduction resumed beneath that margin to produce the main, more voluminous phase of Avalonian arc magmatism (~630–570 Ma). Volcanism and plutonism were accompanied by widespread deposition of volcanogenic turbidites in various volcanic arc basins attributed to an oblique component of the convergence. This phase ended without significant orogenesis at different times across West Avalonia (~590–540 Ma), giving rise to additional rift- and wrench-related basins interpreted in terms of a ridge-trench collision and development of a continental transform fault.

The succession from magmatic arc through transitional arc-rift or wrench basins to stable Cambro-Ordovician platform was adopted with minor age adjustments in the lithotectonic map of Hibbard and others (2006). Available New England data, by then including more reliable U-Pb dates based on small zircon fractions pre-treated for Pb loss (Hepburn and others, 1993; Thompson and others, 1996), placed SE New England magmatic rocks among members of 630 to 580 Ma "younger Neoproterozoic magmatic arc" in figure 1. Overlying the arc complex in the topographic Boston Basin and widening eastward beneath Boston Harbor, Roxbury Conglomerate and argillaceous deposits of the Cambridge Formation constrained by "Vendian" microfossils (Lenk and others, 1982) were assigned to the magmatic arc-to-rift transition sequence.

More accurate and precise crystallization ages now available for Boston-area granites and volcanic rocks (table 1) reinforce cross-terrane correlations with arc-related sequences in more northerly Avalonian terranes (fig. 1). However, a combined chemical abrasion-thermal ionization mass spectrometry [CA-TIMS] and laser ablation-inductively coupled mass spectrometry [LA-ICPMS] approach to dating the Roxbury Conglomerate establishes 595 to 584 Ma U-Pb age constraints that also fall within the interval of arc activity (M. Thompson and others, 2014). Here we present LA-ICPMS and CA-TIMS results indicating that aerially more extensive and much thicker marine deposits of the Cambridge Formation (fig. 2) are significantly younger than the previously reported maximum age of ~570 Ma (Thompson and Bowring, 2000). The new dates suggest a considerable Roxbury-Cambridge depositional hiatus and raise many questions about the tectonic scenario preceding platform deposition in SE New England. Previous correlations with transitional units in more northerly Avalonian terranes must also be re-examined.

EVOLVING VIEWS OF THE CAMBRIDGE FORMATION

Most early observers of sedimentary rocks in the Boston Basin described the typically gray, argillaceous units named for Cambridge, Massachusetts as slate (Shaler, 1869; Crosby, 1888; LaForge, 1932; fig. 2). Cambridge Argillite eventually took hold as

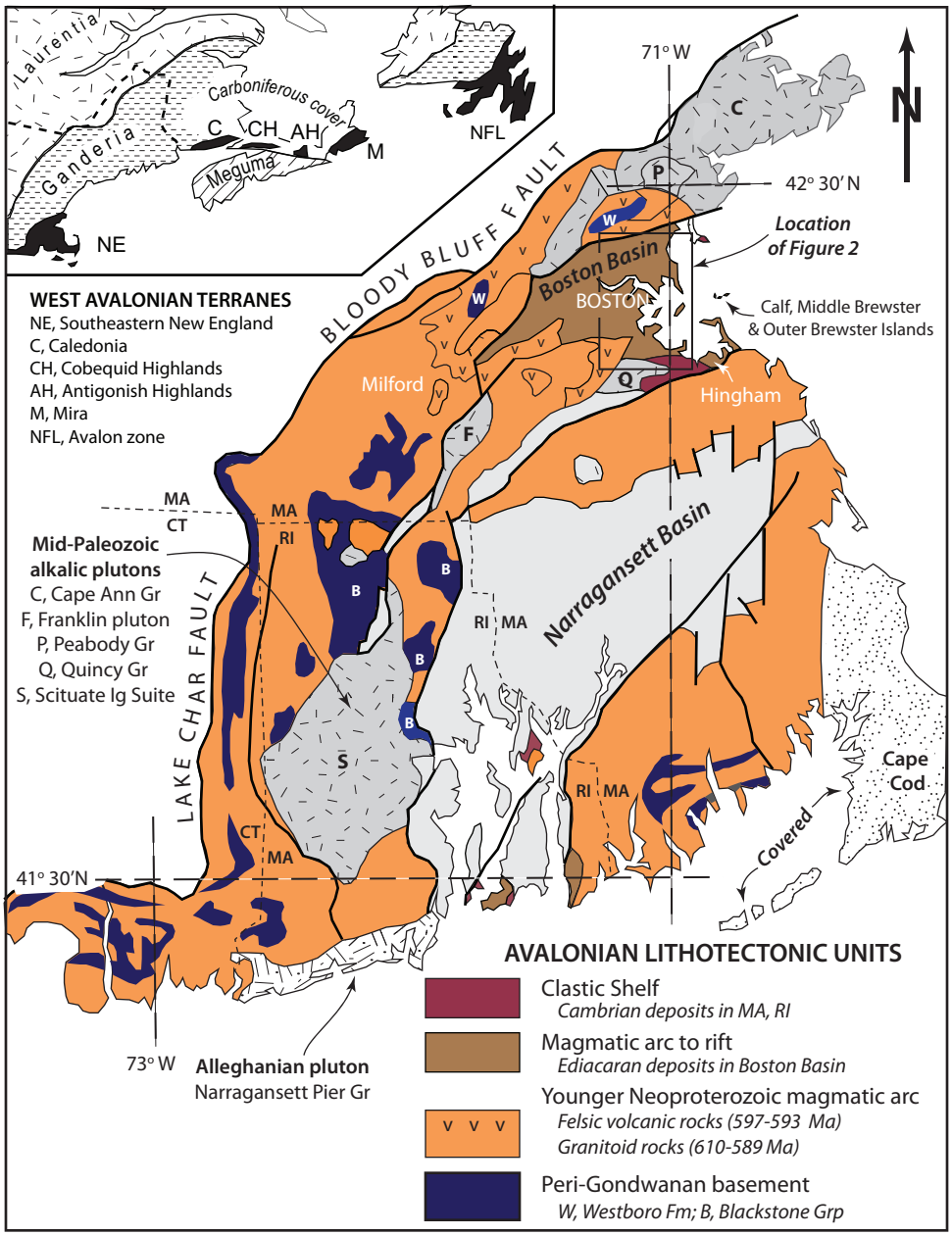

Fig. 1. Simplified geologic map of southeastern New England. Colored units in the legend are based on lithotectonic subdivisions of Hibbard and others (2006). Unlabelled parts of the basement are mainly gneisses of assumed Neoproterozoic age for which U-Pb dates are either unreliable (Zartman and others, 1988) or not available (Murray and others, 1990). Post-Avalonian elements are labelled within the map in shades of gray. The inset map shows other Avalonian terranes mentioned in the text.

the formation name because thin bedding or lamination is more common in these rocks than slaty cleavage (Billings, 1929) and because keeping track of transitions between silty and finer-grained Cambridge units during subsurface mapping is very

TABLE 1

Age constraints on Avalonian arc-related granitoid and volcanic rocks in SE New England

Rock Formation	U-Pb Isotopic Date* (Millions of years)					
	Through 1985†	Current Constraint				
		Lower intercept date	Upper intercept date	$^{207}Pb/^{206}Pb$ date	$^{206}Pb/^{238}U$ date	Source
Brighton Igneous Suite	No data				584.19 ± 0.70	1
					585.37 ± 0.72	"
Dartmouth Pluton	"		595 ± 5			2
Lynn Volcanic Complex	"		596 ± 3			3
					595.8 ± 1.2	4
Mattapan Volcanic	602 ± 3[5]				593.19 ± 0.73	1
Complex				597.4 ± 1.5		4
					596.0 ± 1.4	"
					595.7 ± 1.6	"
			596 ± 2			6
Esmond Granite	621 ± 8[7]				599 ± 2	8
Westwood Granite	no data		599 ± 1			6
Cohasset Granite	"			598.7 ± 1.8		9
Fall River Granite	584 ± 7[10]				604.4 ± 1.2	8
	631 ± 10[10]					
Gneisses						
Ten Rod Gneiss	602 ± 8[11]					
Hope Valley Alaskite	626 ± 19[11]			606 ± 5§		12
Northbridge Gneiss	no data			607 ± 5§		"
Ponagansett Gneiss	"			612 ± 5§		"
Milford Granite	630 ± 15[10]				606.3 ± 1.2	8
Dedham Granite	no data	606 ± 3				3
North of Boston		607 ± 4				"
		609 ± 4				"
				611 ± 2‡		13
Dedham Granite	630 ± 15[10]				608.9 ± 1.2	8
					609.1 ± 1.1	"
					609.5 ± 1.1	"

* *Date* (used throughout the paper to denote what has been measured) is interpreted as crystallization *age*. Unless otherwise indicated, all dates obtained using Thermal Ionization Mass Spectroscopy [TIMS].

† $^{207}Pb/^{206}Pb$ dates for Fall River Granite; other entries in this column are upper intercept U-Pb dates.

§ Obtained via Sensitive High-resolution Ion Microprobe [SHRIMP].

‡ Obtained via Laser Ablation-Inductively Coupled Plasma Mass Spectrometry [LA-ICPMS].

Sources of dates are: 1— Thompson and others, 2014; 2— Hermes and Zartman, 1992; 3— Hepburn and others, 1993; 4—Thompson and others, 2007; 5— Kaye and Zartman, 1980; 6—Thompson and others, 1996; 7—Hermes and Zartman, 1985; 8—Thompson and others, 2010; 9—Dillon and others, 1993 and personal communication of G.R. Dunning; 10—Zartman and Naylor, 1984; 11—Zartman and others, 1988; 12—Walsh and others, 2009; 13—Hanson and McFadden, 2014.

difficult (Rahm, 1962). While recent sedimentological analysis of Cambridge deposits on several Boston Harbor islands (fig. 1) is framed in terms of mudstone, siltstone and fine to very fine sandstone (P. Thompson and others, 2014), *argillite* is retained here as the most convenient name for summarizing Cambridge rock types, especially in subsurface settings detailed below. Recognition of a transitional sequence of argillite

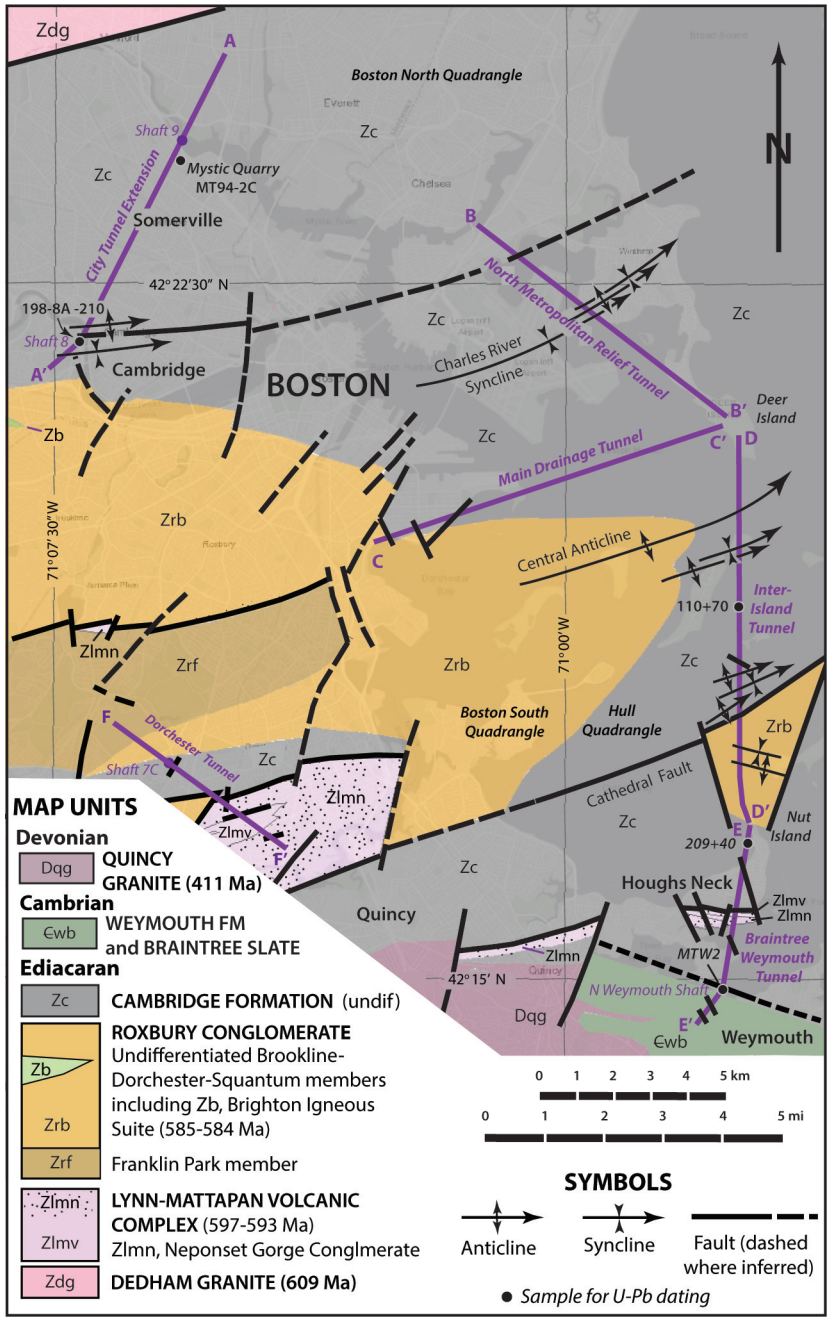

Fig. 2. Simplified geologic map showing distribution of the Cambridge Formation in the vicinity of Boston, Massachusetts and tunnels from which subsurface data were compiled. Cambridge Formation is undifferentiated at this scale, but further divided in figure 3. See figure 1 for location of surface exposures on Calf, Middle Brewster and Outer Brewster islands east of this map in Boston Harbor.

interbedded with quartzose sandstone leading into the lower Cambrian Weymouth Formation on the south margin of the Basin makes *Cambridge Formation* the preferable stratigraphic name.

Surface exposure of the Cambridge Formation in figure 2 is limited to minor, now commonly inaccessible, outcrops in Cambridge and Somerville, Massachusetts north of Boston and in Quincy, Massachusetts to the south. As a result, most previously available information comes from subsurface reports compiled during construction of water supply and sewerage tunnels in the northern parts of the Boston Basin before 1960. Both the City Tunnel Extension (CTE; AA' in fig. 2) and the Main Drainage Tunnel (MDT; CC' in fig. 2) were mapped in detail (Rahm, 1962; Billings and Tierney, 1964), but only one day of reconnaissance was possible in the North Metropolitan Relief Tunnel (NMRT; BB' in fig. 2), so that data from this tunnel was largely obtained from shallow, un-oriented core borings above the tunnel alignment (Billings, 1975). The Dorchester Tunnel completed in 1974 provides a glimpse of the Cambridge Formation on the south side of the Boston Basin (Richardson, 1977; FF' in fig. 2), but the most detailed information from this area comes from the Inter-Island Tunnel (IIT; DD' in fig. 2) and the Braintree-Weymouth Tunnel (BWT; EE' in fig. 2) built in response to a 1986 federal court order to clean up Boston Harbor. Argillite documented on Calf, Middle Brewster and Outer Brewster islands (P. Thompson and others, 2014; fig. 1) during bedrock mapping prior to establishment of the Boston Harbor Islands National Recreation Area in 1996 can also be roughly linked with sections in the tunnels.

Interpretations shown in cross sections of figure 3 have been compiled by the first author from attitudes documented in the early tunnels reports, from unpublished mapping logs of the IIT (Stone & Webster, Inc.) and BWT (GZA Environmental, Inc.), from inspection of surviving core borings archived by the Massachusetts Water Resources Authority, and from traverses of the IIT and BWT in 2000 and 2001 before they were lined. Dimensions related to locations in the tunnels or borehole depths are quoted in feet to correspond with original engineering documents and drilling logs. Samples acquired from core borings and tunnel visits have supplied materials for thin sections used for routine petrography and electron-microbe analysis of constituent minerals, for whole-rock major and trace element geochemical analysis and for U-Pb zircon geochronology via LA-ICPMS and CA-TIMS summarized in the following sections. The synthesis developed below is consistent with all available information, but admittedly permissive. Beyond the greatly expanded database underlying this synthesis, possibilities for sampling the Cambridge Formation are likely to remain spotty.

PETROGRAPHY AND MINERALOGY

Mineralogy throughout the Cambridge sequence is dominated by felty intergrowths of fine silt- to clay-sized white mica and chlorite, accompanied by varying amounts of fragmental quartz and plagioclase, along with phyllosilicate-rich pods interpreted as altered volcanic or argillaceous rock fragments. Such grains typically measure 0.2 to 0.5 mm (coarse silt) but locally reach 1 mm in the fine sand range. Accessory pyrite appears macroscopically, and zircon can be seen in thin section. Electron microprobe analysis reveals chamositic chlorite with Fe/Fe+Mg between 0.60 and 0.75 and K-deficient white mica consistent with illite; plagioclase is uniformly pure albite. Sub-microscopic accessory minerals identified by microprobing include ubiquitous apatite, monazite, rutile and other sulfides (arsenopyrite, galena, chalcopyrite, sphalerite), and in three samples, titanite. Sub-millimeter thick opaque laminae are commonly composed of framboidal pyrite, rutile and/or organic material, but backscatter microprobe images in one sample show a preponderance of Fe-rich chlorite.

In contrast to their mineralogical uniformity, Cambridge deposits show considerable textural variability as illustrated in figure 4. The finest-grained layers are mainly

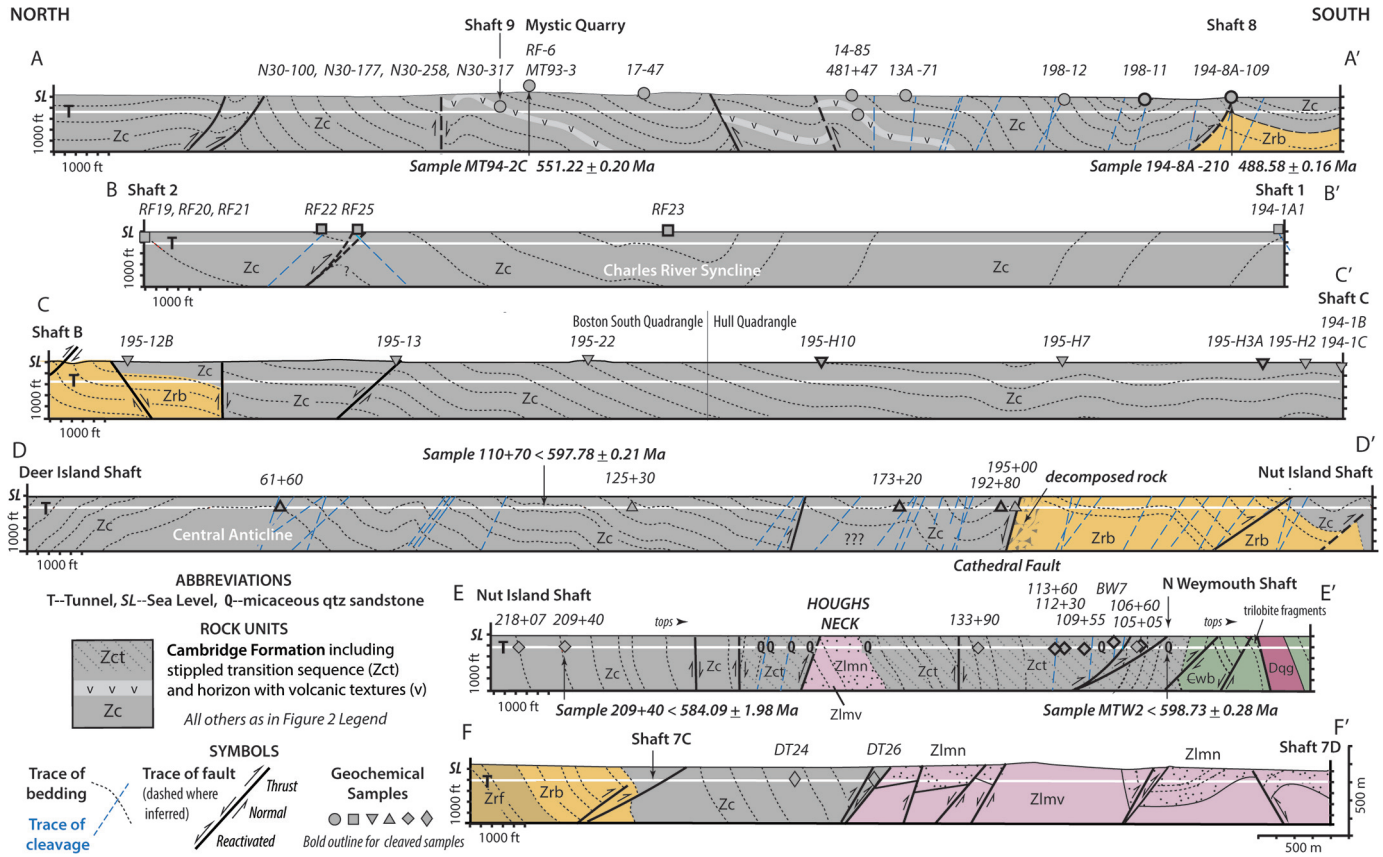

Fig. 3. Structure sections along tunnel alignments shown in figure 2: AA'—City Tunnel Extension, BB'—North Metropolitan Relief Tunnel, CC'—Main Drainage Tunnel, DD'—Inter-Island Tunnel, EE'—Braintree Weymouth Tunnel, FF'—Dorchester Tunnel. Rock units other than the Cambridge Formation are the same as those shown in figure 2 legend. Compositions for geochemical samples are listed in table 2 and are plotted using the same symbols in figure 6A. Summary of U-Pb zircon dates in table 5. Cross sections are scaled in feet to correspond with tunnel mapping logs; a metric scale is shown at lower right.

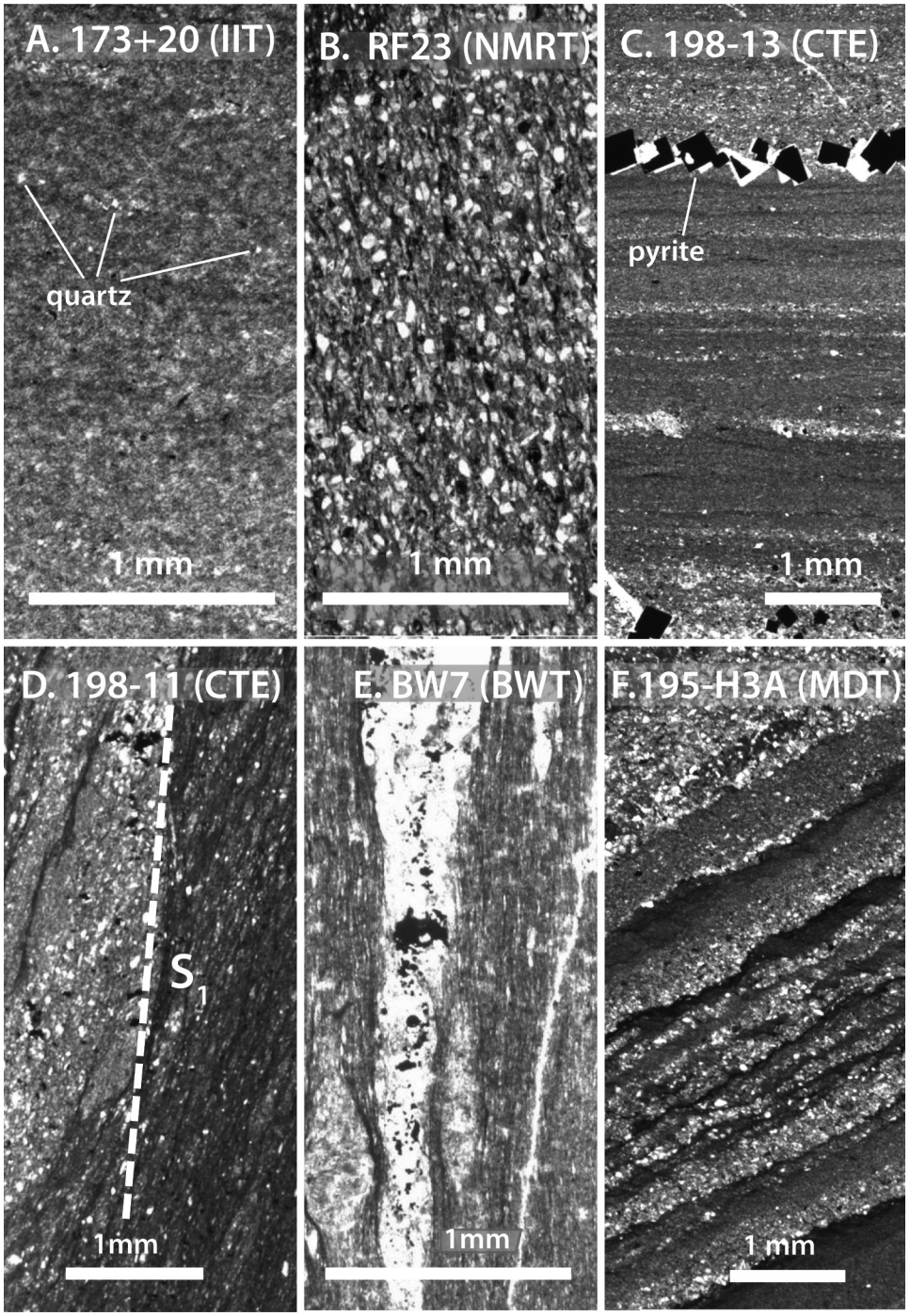

Fig. 4. Plane-light photomicrographs of textures in Cambridge argillite in Boston-area tunnels. (A) Crystal-poor (<25 modal % quartz + plagioclase). (B) Crystal rich. (C) Bedding laminae with indistinct contacts. (D) Bedding truncated and displaced parallel to cleavage (S_1). North to left. (E) Bedding transposed parallel to cleavage. (F) Graded bedding. IIT—Inter-Island Tunnel, NMRT—North Metropolitan Relief Tunnel, CTE—City Tunnel Extension, BWT—Braintree Weymouth Tunnel, MDT—Main Drainage Tunnel.

composed of chlorite and illite with <10 modal percent fragments of quartz and plagioclase (fig. 4A). The coarsest layers contain 20 to 25 modal percent quartz + plagioclase varying from rounded to angular in shape. The distinctly grainy appearance of such samples is enhanced by an equal abundance of altered lithic fragments in the form of irregular pods that are typically difficult to distinguish from surrounding phyllosilicate-rich matrix (fig. 4B). Many samples contain alternations between coarser and finer laminae across indistinct contacts, with some laminae measuring only a few crystal diameters (fig. 4C). In fault zones or in hinge areas of folds, silty beds may be truncated and translated parallel to cleavage (S_1 in fig. 4D) or completely transposed (fig. 4E). Grading is also common in Cambridge samples as illustrated in figure 4F where coarsest quartz grains reach into the fine sand range (~0.15 mm).

A 300' drill core at Shaft 9 of the City Tunnel Extension (fig. 2) contains numerous samples showing textures consistent with volcanic origin. Several of these are illustrated in figure 5. The rock at depth −28.5 ft was sampled from a ~4 ft (1.2 m) thick layer of mafic porphyry containing abundant <0.5 mm sericitized plagioclase laths aligned in a phyllosilicate-rich matrix (fig. 5A). The turbid brownish color of the matrix in plane light is consistent with considerable Fe-rich chlorite. In contact with the host crystal-poor argillite, an altered glassy rind retains vestiges of a tubular, possibly scoriaceous texture (fig. 5B). The irregular interpenetrating contact between argillite and a thiner porphyry sampled lower in the core suggest interaction between lava and soft sediment (fig. 5C). Possible accretionary lapilli or pumice clasts in the form of flattened crystal-free phyllosilicate domains tapering into the matrix (fig. 5D) are present at several depths, and embayed quartz appears in a crystal-rich layer at -165.62 ft (fig. 5E).

GEOCHEMISTRY

Whole-rock geochemistry provides the most convenient means of characterizing Cambridge compositions and comparing them across the Boston Basin. Available data include whole-rock major and trace element analyses listed in table 2. Penetrative cleavage observed in 15 of 45 analyzed samples (symbols with bold outline in figs. 3 and 6A) raise questions about mobility of CaO, Na_2O and K_2O and whether measured concentrations of these reliably reflect depositional compositions. However, in figure 6A adapted from a diagram developed by Garrels and Mackenzie (1971, p. 213) to represent the full chemical range of "average" modern sediments, cleaved Cambridge samples span the same compositional range as the majority of samples that lack cleavage. Compositions for reference clays from the original diagram as well as the North American shale composite (NASC of Gromet and others, 1984) lie on the same trajectory, suggesting that strain-related alkali mobility (Wintsch and others, 1991, for example) has not significantly altered the compositions of these rocks.

Cambridge silica contents lie with few exceptions between 60 and 70 weight percent SiO_2 (table 2), consistent with reference compostions in figure 6A (data re-calculated volatile-free from Clarke, 1924; El Wakeel and Riley, 1961; Hirst, 1962; Gromet and others, 1984). By contrast, Cambridge compositions are commonly richer than reference muds in Al_2O_3 and K_2O, so that points plot in a broad band that sweeps into the lower left corner of figure 6A. Illite compositions from bentonitic sediments (table 2–16 in Weaver, 1989, calculated volatile-free) likewise fall into that area, in line with the previous suggestion (Thompson and Bowing, 2000) that Cambridge deposits include a component of volcanic ash. Terrigenous detritus is the obvious candidate for the other end member of this mixture.

The geochemical composition of upper continental crust which supplies terrigenous detritus to marine basins (overview in Taylor and McLennan, 1985) is typically approximated using rare earth element [REE] concentrations in fine grained terrestrial deposits, but major element data are also available in some cases. Included in

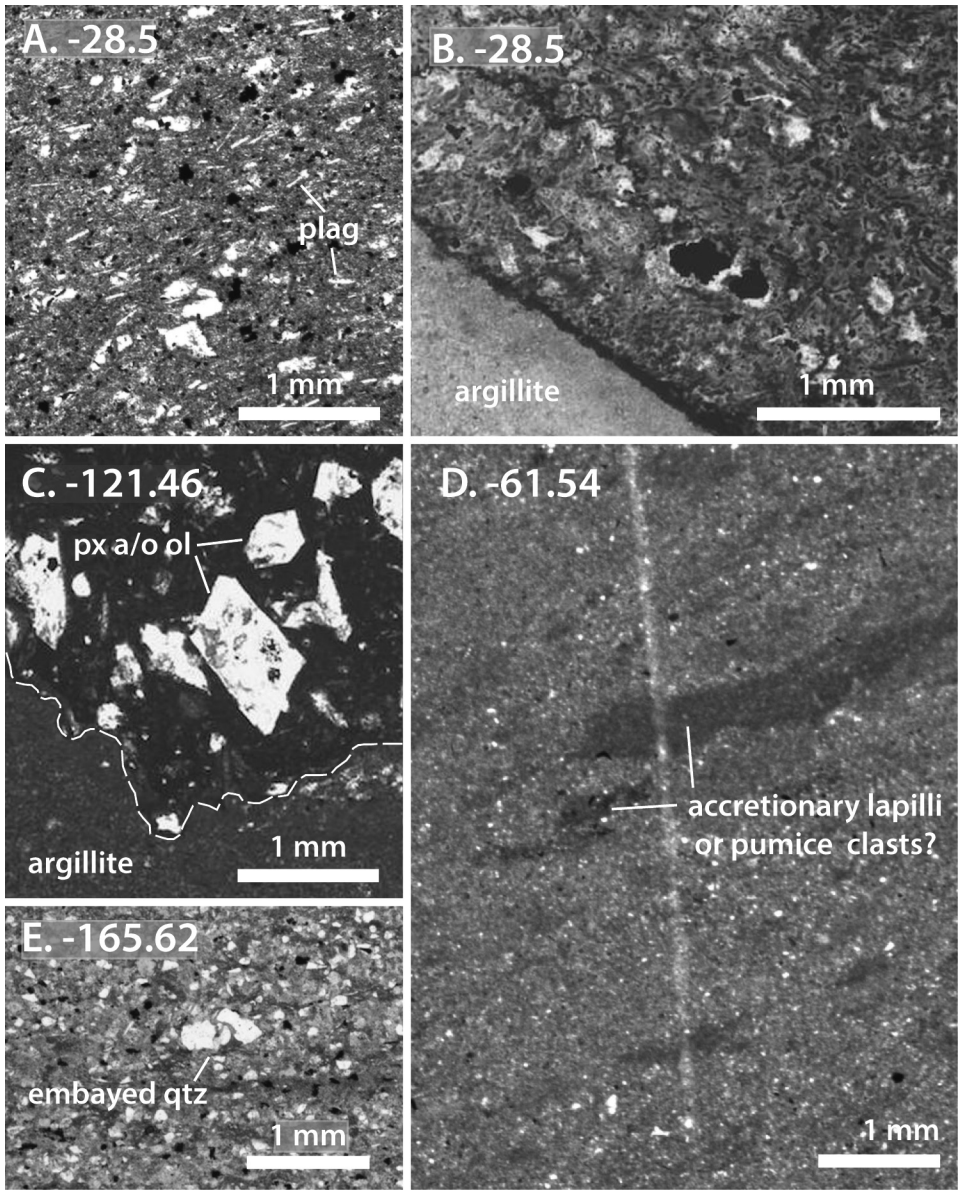

Fig. 5. Plane-light photomicrographs showing volcanic textures in samples City Tunnel Extension Shaft 9. (A) Plagioclase (plag) phenocrysts in mafic porphyry. (B) Chilled margin in porphyry in contact with argillite. (C) Loaded porphyry-argillite contact. Labelled grains are pseudomorphed pyroxene (px) and/or olivine (ol). (D) Phyllosilicate-rich domains interpreted as flattened accretionary lapilli or pumice clasts. (E) Embayed volcanic quartz grains.

figure 6A are ratios calculated from New Zealand loess sampled from the Banks Peninsula of New Zealand's South Island (Taylor and others, 1983). These cluster on the right edge of the diagram at the end of a proposed mixing line that terminates among illite compositions on the lower left. The NASC average shows higher calcium and potassium than most argillite samples, but plots towards the terrigenous end of the

TABLE 2

Major and trace element compositions of samples from the Cambridge Formation

	1	2	3	4	5	6	7	8	9	10	11	12	13	14	15
	MQ		CTE											NMRT	
Field #	RF-6*	MT 93-3*	N30-100*	N30-177*	N30-258*	N30-317*	17- 47*	14-85*	481+47§	13A-71*	198-12	198-11	194-8A-109	RF19*	RF20
								Major elements (weight %)							
SiO_2	62.26	58.27	63.49	62.9	61.35	61.17	55.15	63.01	54.68	63.15	64.46	63.28	64.26	68.09	65.64
TiO_2	1.45	1.79	0.92	1.00	1.07	1.08	2.14	0.94	0.72	1.05	0.80	0.85	0.91	1.13	1.13
Al_20_3	19.61	21.22	18.41	20.71	20.11	19.08	21.86	20.13	20.74	19.1	19.36	19.51	19.87	19.92	18.88
Fe_2O_3†	7.97	8.93	6.43	6.4	8.56	8.3	12.43	6.62	7.94	7.92	6.90	8.13	6.44	4.76	8.21
MnO	0.1	0.12	0.11	0.05	0.13	0.14	0.22	0.07	0.15	0.1	0.20	0.17	0.13	0.07	0.20
MgO	2.01	2.29	1.73	1.23	1.73	1.69	1.53	1.92	0.45	1.6	2.26	2.23	1.98	1.27	1.80
CaO	0.57	0.76	0.79	0.97	1.39	1.06	1.43	0.37	0.41	0.92	0.58	0.80	0.46	0.46	0.44
Na_2O	0.64	2.79	1.79	1.14	1.69	1.2	1.4	1.45	2.28	1.67	2.91	1.75	2.12	0.15	0.11
K_2O	3.33	3.39	3.17	4.04	3.37	2.87	3.64	5.29	4.72	2.73	2.65	3.23	3.57	3.55	3.10
P_2O_5	0.16	0.18	0.08	0.57	0.08	0.07	0.3	0.12		0.11	0.09	0.32	0.15	0.15	0.22
Total‡	98.10	99.74	96.92	99.01	99.48	96.66	100.1	99.92	92.09	98.35	100.21	100.27	99.89	99.55	99.73
								Trace elements (ppm)							
Nb	14	17	34	17	14	11	14	20		12	13.7	14.3	14.8	13	16.1
Zr	226	230	203	231	209	198	240	216		210	218	214	225	224	277
Y	40	51	15	45	32	29	48	25		32	32.6	38.8	48.7	39	43.1
Sr	90	101	111	113	111	109	225	58		84	199	114	88	59	50
U											3	3	4		3
Rb	106	105	115	140	119	93	107	188		89	97.6	120.9	129.3	109	100.6
Th											10	10	11		10
Pb											39	9	46		2
Ga											22	23	23		22
Zn	63	77	76	78	79	107	102	73		90	106	140	86	40	57
Ni	24	24	27	22	30	25	26	34		20	37	36	35	27	30
Cr											61	61	71		73
V											116	132	142		123
Ce	63	89	68	56	89	51	78	45		65	56	74	53	70	60
Ba	744	687	570	759	735	709	616	788		612	733	635	710	858	767
La	36	52	28	18	45	19	30	8		2	25	35	23	20	24

* Analyses from University of Rhode Island XRF Lab; all other analyses except 481+47 from the Ronald B. Gilmore X-ray Analytical Facility, University of Massachusetts.
§ Wet chemical anaysis of Billings and Tierney (1964).
† Total iron.
‡ Volatile-free.
Abbreviations: MQ—Mystic Quarry, CTE—City Tunel Extension, NMRT—North Metropolitan Relief Tunnel.

TABLE 2
(continued)

	16	17	18	19	20	21	22	23	24	25	26	27	28	29	30
		NMRT				MDT									IIT
Field #	RF21*	RF22	RF23	RF25	194-1A1	195-12B	195-13	195-22	195-H10	195-H7	195-H3A*	195-H2	194-1B	194-1C	61+60*
	Major elements (weight %)														
SiO_2	65.96	63.57	65.65	67.78	70.00	66.28	61.72	66.12	63.57	65.48	64.10	65.08	64.53	65.12	66.64
TiO_2	1.01	0.83	0.79	0.83	0.86	0.60	0.85	0.93	0.99	1.00	1.08	1.02	1.06	1.01	0.76
Al_2O_3	18.97	20.59	17.18	17.21	17.63	18.07	16.83	18.31	19.51	18.48	18.41	19.37	17.34	19.76	18.40
Fe_2O_3†	7.86	6.64	8.73	6.30	5.48	5.34	7.19	6.57	7.71	7.03	8.59	7.71	6.99	2.65	5.57
MnO	0.18	0.14	0.17	0.12	0.09	0.14	0.16	0.13	0.13	0.13	0.22	0.16	0.19	0.12	0.17
MgO	2.11	1.83	2.58	1.86	1.69	1.85	2.44	2.12	2.30	2.27	2.48	2.17	1.83	1.98	1.48
CaO	0.44	0.47	1.04	0.34	0.31	1.89	4.20	0.62	0.37	0.85	1.63	0.74	3.20	0.39	1.43
Na_2O	0.33	0.97	1.49	2.38	0.42	2.49	2.37	2.31	1.84	1.84	0.45	0.57	1.94	1.68	2.27
K_2O	3.01	4.24	2.32	2.50	3.01	2.80	2.34	2.69	3.05	2.78	2.90	3.05	2.54	3.24	2.99
P_2O_5	0.13	0.26	0.10	0.11	0.14	0.12	2.02	0.17	0.19	0.13	0.17	0.18	0.35	0.17	0.27
Total‡	100.00	99.54	100.05	99.43	99.63	99.58	100.12	99.97	99.66	99.99	100.03	100.05	99.97	96.12	99.98
	Trace elements (ppm)														
Nb	17.0	21.8	11.9	13.0	3.8	15.4	12.1	15.5	14.6	16.1	15.0	15.5	14.9	15.7	14
Zr	219	231	260	224	115	231	193	260	223	234	203	231	230	258	200
Y	43.0	28.6	32.3	27.7	12.8	38.0	57.3	38.8	30.2	42.6	37.0	32.1	37.5	42.9	48
Sr	52	80	134	157	1626	196	232	127	102	124	91	91	143	98	89
U		4	2	2	1	4	2	3	3	3		3	2	3	
Rb	102.0	158.9	76.1	91.0	19.3	103.7	81.9	96.6	107.7	99.9	99.0	105.3	89.5	115.9	115
Th		16	9	8	1	14	8	10	9	9		8	8	10	
Pb		19	8	5	11	64	19	19	11	18		4	15	11	
Ga		24	20	20	20	21	20	23	23	23		23	19	24	
Zn	70	100	89	97	69	88	88	109	98	121	87	94	85	86	87
Ni	28	30	32	26	50	30	36	30	37	31	39	32	25	27	53
Cr		60	59	51	65	31	63	56	58	56		57	61	52	
V		104	86	109	136	89	114	109	117	112		121	111	115	
Ce	67	52	61	44	33	117	55	65	56	61	74	42	62	58	98
Ba	812	692	597	611	393	644	515	638	683	670	634	706	580	741	694
La	32	21	24	18	13	50	20	28	25	25	44	18	26	24	14

* Analyses from University of Rhode Island XRF Lab; all other analyses from the Ronald B. Gilmore X-ray Analytical Facility, University of Massachusetts.
† Total iron.
‡ Volatile-free.
Abbreviations: NMRT—North Metropolitan Relief Tunnel, MDT—Main Drainage Tunnel, IIT—Inter-Island Tunnel.

TABLE 2
(continued)

	31	32	33	34	35	36	37	38	39	40	41	42	43	44	45
	IIT				BWT									DT	
Field #	125+30	173+20*	192+80*	195+00	218+07	209+40	133+90	113+60	112+30	109+55	BW7	106+60	105+05	DT24	DT26*
	Major elements (weight %)														
SiO_2	66.55	60.18	64.41	62.42	66.36	66.24	64.85	66.11	66.09	55.81	61.57	60.78	62.41	67.17	63.35
TiO_2	0.76	1.02	0.85	1.10	0.79	1.00	1.01	1.05	1.14	1.52	0.91	1.51	1.34	0.94	1.03
Al_2O_3	18.47	21.01	19.08	22.61	18.01	17.28	18.71	16.59	17.79	22.81	21.42	21.29	20.26	15.65	17.37
Fe_2O_3†	5.54	7.09	7.76	6.22	6.65	6.15	6.22	8.25	7.48	12.43	9.23	9.57	9.34	5.87	8.36
MnO	0.18	0.09	0.17	0.17	0.13	0.15	0.10	0.16	0.11	0.19	0.14	0.12	0.11	0.12	0.13
MgO	1.50	1.81	1.53	1.66	1.96	1.92	1.87	1.56	1.61	2.43	2.23	1.72	1.66	1.65	2.22
CaO	1.44	1.22	1.76	0.22	1.10	2.03	0.74	1.73	0.51	0.56	0.15	0.12	0.12	0.91	1.03
Na_2O	2.28	0.39	0.4	0.15	1.83	2.75	2.36	1.98	2.24	1.22	0.78	1.42	1.54	1.82	0.99
K_2O	2.96	3.65	3.45	5.31	3.03	2.50	3.43	2.38	2.71	2.86	3.00	3.36	3.15	2.81	2.63
P_2O_5	0.27	0.62	0.15	0.15	0.15	0.19	0.12	0.08	0.10	0.41	0.09	0.04	0.03	0.11	0.24
Total‡	99.95	97.08	99.56	100.01	100.01	100.21	99.41	99.89	99.78	100.24	99.52	99.93	99.96	97.05	97.35
	Trace elements (ppm)														
Nb	15.0	15	14	20.9	13.5	14.0	14.0	10.2	13.7	15.4	10.2	15.9	14.7	19.7	11
Zr	194	236	200	347	214	252	262	203	254	263	203	256	238	318	205
Y	23.3	34	30	49.5	26.0	34.4	35.2	32.1	26.6	42.1	32.1	37.8	35.2	27.6	32
Sr	166	363	104	159	126	187	151	178	196	217	178	161	151	86	126
U	3			2	2	2	2	1	1	1	1	2	1	2	
Rb	112.5	144	116	170.7	106.4	88.5	123.2	81.3	94.8	110.1	81.3	137.6	129.6	134.3	97
Th	11			12	10	8	8	5	8	10	5	8	8	11	
Pb	15			22	11	11	12	6	17	14	6	2	2	5	
Ga	21			27	21	21	24	19	20	27	19	24	23	16	
Zn	102	108	88	99	86	99	101	103	87	130	103	125	120	50	62
Ni	24	32	35	24	28	28	26	10	12	35	10	31	29	14	28
Cr	49			44	49	62	56	30	30	80	30	79	78	45	
V	95			98	107	118	118	111	108	219	111	209	196	65	
Ce	54	51	68	69	45	72	69	41	34	57	41	58	60	70	67
Ba	733	708	503	816	677	681	797	555	533	402	555	759	716	553	657
La	15.0	15	14	20.9	23	34	29	17	14	23	17	23	24	29	27

* Analyses from University of Rhode Island XRF Lab; all other analyses from the Ronald B. Gilmore X-ray Analytical Facility, University of Massachusetts.
† Total iron.
‡ Volatile-free.
Abbreviations: IIT—Inter-Island Tunnel, BWT—Braintree Weymouth Tunnel, DT—Dorchester Tunnel.

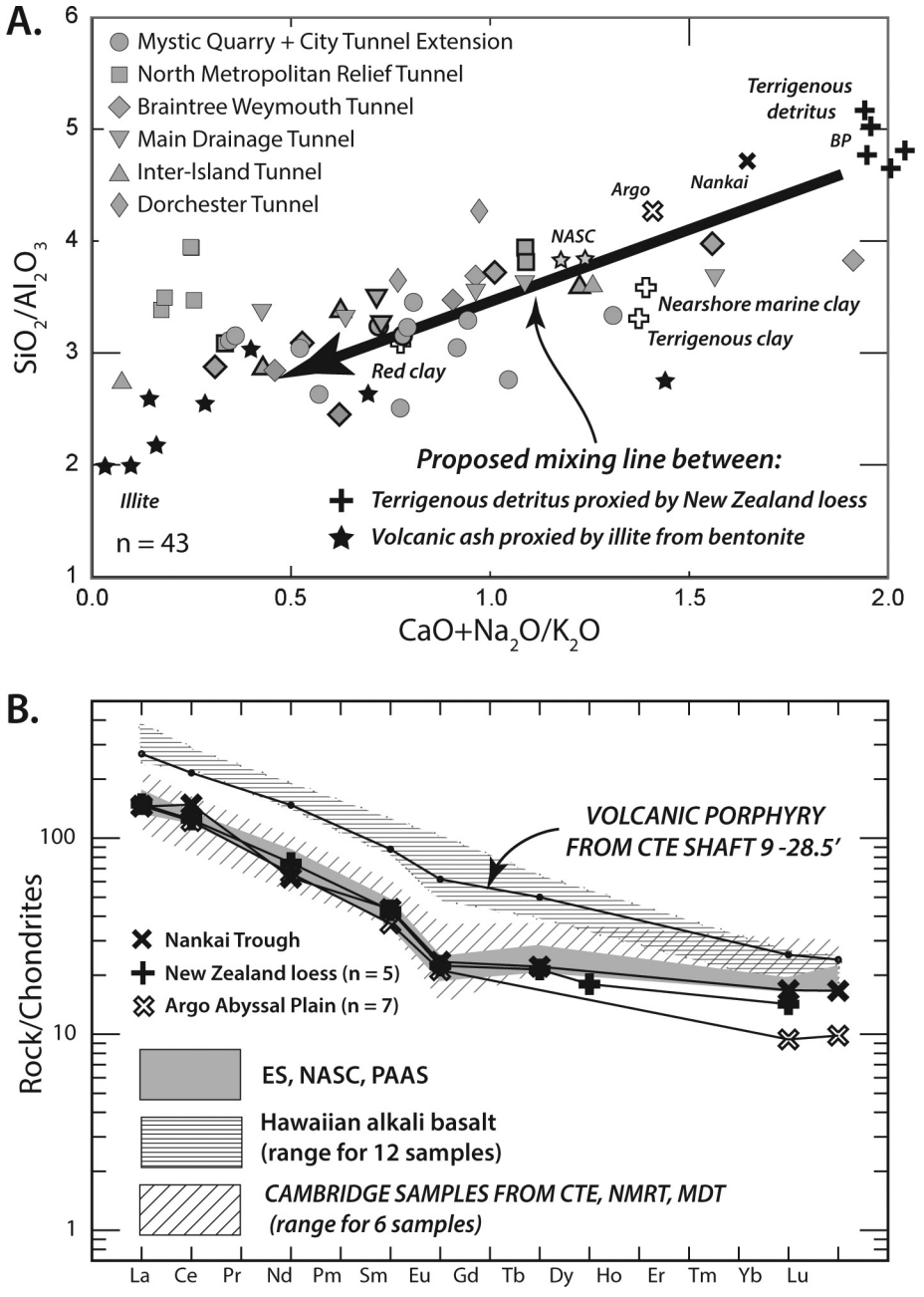

Fig. 6. Whole-rock geochemistry of the Cambridge Formation. (A) Argillite composition compared to modern marine sediments (plotted after Garrrels and Mackenzie, 1971). Symbols with bold outlines denote samples with cleavage. Analyses 22, 28 in table 2 contain >3 wt % CaO and plot outside the field on the right. (B) REE compositions. Normalization factors from Sun and McDonough (1989). Sources of reference compositions: Nearshore marine clay—Hirst (1962), terrigenous clay—Clarke (1924), red clay—El Wakeel and Riley (1961), illite from bentonite—Weaver (1989), New Zealand loess—Taylor and others (1983), Argo Abyssal Plain—Plank and Ludden (1992), Nankai Trough—Underwood and Pickering (1996), Hawaiian alkali basalt—Spengler and Garcia (1988). CTE—City Tunnel Extension, NMRT—North Metropolitan Relief Tunnel, MDT—Main Drainage Tunnel.

TABLE 3

Rare Earth Element [REE] compositions of representative samples from the Cambridge Formation

	Mystic Quarry		CTE			MDT	NMRT
	MT93-3	RF6	Shaft 9 -28.5 ft	Shaft 9 -61.5 ft	Shaft 9 -135 ft	195-H3A	RF21
La	43.4	25.1	63.8	51.4	27.3	31.9	33.0
Ce	86.4	50.5	131.8	96.2	57.2	68.2	75.2
Nd	463	26.6	68.9	47.0	25.1	33.1	34.9
Sm	8.65	5.21	13.44	9.15	5.71	7.07	8.05
Eu	2.17	1.42	3.58	2.12	0.83	1.49	1.75
Gd	8.3	5.9	12.5	7.2	5.0	6.5	8.5
Tb	1.38	0.99	1.87	1.12	0,77	1.08	1.37
Tm	0.73	0.63	0.68	0.52	0.44	0.54	0.73
Yb	5.24	4.54	4.32	3,62	3.06	3.81	5.03
Lu	0.77	0.70	0.61	0.53	0.44	0.57	0.73

Instrumental neutron activation analyses [INAA] courtesy of Nelson Eby, Department of Earth Sciences, University of Massachusetts Lowell. Methods detailed in Eby and others (1998).

Cambridge spectrum. Seafloor deposits of terrestrial derivation documented in settings including the Nankai accretionary prism of southwest Japan (ODP Site 808; Underwood and Pickering, 1996) and the Argo Abyssal Plain adjacent to northwest Australia (ODP Site 765; Plank and Ludden, 1992; Plank and Langmuir, 1998) also plot on the right side of figure 6A.

The presence of terrigenous components in Cambridge argillite is also consistent with REE patterns obtained from six samples from the CTE, MDT and NMRT (table 3). All of these show light REE enrichment, a mild Eu anomaly and a flat heavy REE distribution quite similar to values both from the New Zealand loess and the two ODP sites (fig. 6B). The gray field in figure 6B encompassing patterns for average continental crust based on the NASC as well as the Post-Archean average Australian Shale (PAAS of Nance and Taylor, 1976) and European shale composite (ES of Haskin and Haskin, 1966) also lies within the hatched Cambridge envelope. A more enriched REE pattern was obtained from core boring113-N30 −28.5 from CTE Shaft 9. This sample contains abundant plagioclase laths of probable volcanic origin (fig. 5A), and its REE distribution falls within the range shown by alkali basalt from Hawaii's Kohala Volcano (Spengler and Garcia, 1988; horizontally ruled field in fig. 6B).

U-Pb GEOCHRONOLOGY

Samples for U-Pb zircon dating were collected from five locations shown in both the map of the study area (fig. 2) and accompanying cross sections (fig. 3). Zircon was separated from crushed samples via Wilfley table, Frantz magnetic separator and heavy liquids. Stratified samples MT94-2C and MTW2 yielded abundant zircon of sufficient size for LA-ICPMS investigation of age spectra. The youngest grains identified by these analyses were then removed from the epoxy mounts and re-dated via CA-TIMS to obtain precise $^{206}Pb/^{238}U$ dates. Low zircon yield and small size proved too small for this approach in samples 110 + 70 and 209 + 40, so these were analyzed by CA-TIMS only. For igneous sample 198-8A-210 which yielded a single zircon population, only CA-TIMS was necessary. Details of sample preparation and analysis for each method as well as an explanation of ± x/y/z error reporting can be found in the Appendix. Cathodoluminescence [CL] images and LA-ICPMS isotopic data are included as Supplementary Data (Appendix fig. A1 and Appendix table A1, respectively). CA-TIMS isotopic data appear in table 4. Sections below contain details about and results from each sample, and all dates and errors are summarized in table 5.

TABLE 4

CA-TIMS U-Pb isotopic data

									Radiogenic Isotope Ratios								Isotopic Dates					
LA-ICPMS		Tracer	Th	^{206}Pb*	mol %	Pb*	Pb_c	$\frac{^{206}Pb}{^{204}Pb}$	$\frac{^{208}Pb}{^{206}Pb}$	$\frac{^{207}Pb}{^{206}Pb}$	% err	$\frac{^{207}Pb}{^{235}U}$	% err	$\frac{^{206}Pb}{^{238}U}$	% err	corr.	$\frac{^{207}Pb}{^{206}Pb}$		$\frac{^{207}Pb}{^{235}U}$		$\frac{^{206}Pb}{^{238}U}$	
Sample	label	solution	U	x10^{-13} mol	^{206}Pb*	Pb_c	(pg)									coef.		±		±		±
(a)	(b)	(c)	(b)	(c)	(c)	(c)	(c)	(d)	(e)	(e)	(f)	(e)	(f)	(e)	(f)		(g)	(f)	(g)	(f)	(g)	(f)
MT94-2C Mystic Quarry ash bed, Somerville, MA (UTM coordinates: 19T 03 27 667 E, 46 95 589 N)*																						
z1	5, 42	ET535	0.613	0.3793	99.43%	54	0.18	3170	0.191	0.058542	0.178	0.720681	0.227	0.089324	0.073	0.764	549.13	3.88	551.07	0.97	551.54	0.39
z3	11, 79	ET535	0.617	0.0759	95.98%	7	0.26	449	0.192	0.058244	0.950	0.716750	1.037	0.089291	0.198	0.518	537.98	20.79	548.75	4.40	551.34	1.05
z4	6, 56	ET535	1.368	0.0941	97.16%	13	0.23	636	0.427	0.058255	0.728	0.717595	0.804	0.089381	0.170	0.533	538.37	15.92	549.25	3.41	551.87	0.90
z5	7, 66	ET535	0.774	0.3060	99.27%	44	0.19	2468	0.241	0.058487	0.181	0.719217	0.229	0.089227	0.078	0.717	547.07	3.96	550.20	0.97	550.96	0.41
z6	13,99	ET535	1.251	0.1691	98.52%	24	0.21	1222	0.390	0.058437	0.366	0.718835	0.416	0.089255	0.102	0.579	545.22	8.00	549.98	1.77	551.13	0.54
z7	10, 78	ET535	0.516	0.2782	99.12%	34	0.21	2043	0.161	0.058628	0.263	0.721284	0.307	0.089267	0.095	0.582	552.34	5.74	551.42	1.31	551.20	0.50
z8	37	ET535	1.149	0.1730	98.68%	26	0.19	1371	0.359	0.058491	0.365	0.719027	0.418	0.089197	0.116	0.573	547.22	7.96	550.09	1.78	550.79	0.61
194-8A-210 Aplite sill, CTE Shaft 8 (UTM coordinates: 19T 03 25 498 E, 46 92 140 N)*																						
z1		ET535	0.570	0.5511	99.66%	90	0.16	5308	0.178	0.056989	0.112	0.617719	0.163	0.078649	0.071	0.826	490.12	2.47	488.42	0.63	488.05	0.33
z2		ET535	0.536	0.5123	99.57%	71	0.18	4229	0.168	0.056991	0.131	0.618713	0.186	0.078772	0.085	0.784	490.21	2.88	489.04	0.72	488.79	0.40
z3		ET535	0.460	0.6038	99.67%	90	0.17	5439	0.144	0.057010	0.148	0.618984	0.191	0.078781	0.073	0.715	490.93	3.27	489.21	0.74	488.84	0.34
z4		ET535	0.630	0.3900	99.50%	62	0.16	3624	0.197	0.056954	0.138	0.616573	0.188	0.078551	0.071	0.793	488.76	3.06	487.70	0.73	487.47	0.33
z5		ET535	0.541	0.7784	99.70%	100	0.20	5925	0.169	0.057029	0.109	0.618751	0.165	0.078725	0.080	0.822	491.67	2.40	489.06	0.64	488.51	0.37
z6		ET535	0.509	1.4627	99.61%	76	0.48	4568	0.159	0.056928	0.108	0.617553	0.160	0.078712	0.067	0.858	487.75	2.38	488.31	0.62	488.43	0.31
z7		ET535	0.480	0.2263	99.01%	30	0.19	1828	0.150	0.056954	0.273	0.617686	0.320	0.078694	0.083	0.657	488.74	6.02	488.40	1.24	488.32	0.39
MTW2, Micaceous quartzose sandstone, BWT North Weymouth Shaft (UTM coordinates: 19T 03 38 005 E, 46 78 742 N)*																						
z1a	336	ET2535	0.904	0.6715	98.94%	31	0.60	1694	0.281	0.059981	0.119	0.806081	0.152	0.097512	0.055	0.716	601.91	2.58	600.25	0.69	599.81	0.31
z1b	336	ET2535	0.949	0.6291	99.35%	51	0.34	2769	0.295	0.059939	0.153	0.805276	0.204	0.097483	0.119	0.666	600.41	3.32	599.80	0.93	599.64	0.68
z2a	277	ET2535	0.987	0.6719	99.45%	62	0.31	3304	0.307	0.060082	0.135	0.806337	0.171	0.097380	0.090	0.625	605.55	2.91	600.40	0.78	599.03	0.51
z2b	277	ET2535	0.829	0.7625	99.41%	55	0.37	3073	0.258	0.059892	0.139	0.803231	0.160	0.097311	0.054	0.540	598.71	3.00	598.65	0.72	598.63	0.31
z3	340	ET2535	0.644	0.8861	99.39%	51	0.46	2932	0.200	0.060227	0.108	0.821776	0.128	0.099004	0.046	0.569	610.78	2.34	609.04	0.58	608.57	0.27
z4	313	ET2535	0.542	2.1697	99.83%	179	0.31	10619	0.168	0.060225	0.036	0.822176	0.069	0.099055	0.046	0.875	610.71	0.79	609.26	0.32	608.87	0.27
z5	310	ET2535	0.532	0.8478	99.62%	81	0.27	4788	0.165	0.060228	0.072	0.823380	0.095	0.099196	0.044	0.688	610.81	1.55	609.93	0.43	609.69	0.26
z6	318	ET2535	0.564	1.4795	99.69%	100	0.38	5895	0.176	0.060233	0.056	0.823923	0.076	0.099253	0.036	0.720	610.99	1.22	610.23	0.35	610.03	0.21
110+70 Cambridge argillite, Inter-Island Tunnel (UTM coordinates: 19T 03 38 614 E, 46 86 982 N)*																						
z1		ET2535	0.954	0.4564	99.62%	89	0.14	4763	0.296	0.060443	0.167	0.837292	0.195	0.100514	0.097	0.518	618.49	3.59	617.65	0.90	617.42	0.57
z2		ET2535	0.622	0.9010	99.78%	143	0.16	8290	0.193	0.060481	0.101	0.838643	0.131	0.100613	0.073	0.651	619.85	2.17	618.40	0.61	618.00	0.43
z3		ET2535	0.544	1.2127	99.74%	117	0.26	6898	0.169	0.060194	0.055	0.821030	0.077	0.098970	0.037	0.750	609.57	1.19	608.62	0.35	608.37	0.21
z5		ET2535	1.174	1.0062	99.77%	153	0.19	7793	0.365	0.059832	0.071	0.801226	0.086	0.097166	0.037	0.598	596.53	1.53	597.52	0.39	597.78	0.21
z6		ET2535	0.922	0.2451	99.04%	35	0.20	1883	0.287	0.059951	0.305	0.803740	0.342	0.097277	0.086	0.531	600.84	6.61	598.94	1.55	598.43	0.49

TABLE 4
(continued)

									Radiogenic Isotope Ratios									Isotopic Dates					
Sample	LA-ICPMS label	Tracer solution	Th/U	$^{206}Pb^*$ x10^{-13} mol	mol % $^{206}Pb^*$	Pb^*/Pb_c	Pb_c (pg)	$^{206}Pb/^{204}Pb$	$^{208}Pb/^{206}Pb$	$^{207}Pb/^{206}Pb$	% err	$^{207}Pb/^{235}U$	% err	$^{206}Pb/^{238}U$	% err	corr. coef.	$^{207}Pb/^{206}Pb$	±	$^{207}Pb/^{235}U$	±	$^{206}Pb/^{238}U$	±
(a)	(b)	(c)	(b)	(c)	(c)	(c)	(c)	(d)	(e)	(e)	(f)	(e)	(f)	(e)	(f)		(g)	(f)	(g)	(f)	(g)	(f)
209+40 Cambridge argillite, Braintree Weymouth Tunnel (UTM coordinates: 19T 03 38 768 E, 46 82 036 N)*																							
z1		ET2535	0.657	0.1749	99.12%	36	0.13	2055	0.204	0.060687	0.306	0.856118	0.332	0.102360	0.098	0.396	627.20	6.60	628.00	1.55	628.22	0.59
z2		ET2535	0.642	0.3128	98.37%	19	0.43	1105	0.200	0.060464	0.295	0.842543	0.324	0.101108	0.053	0.595	619.26	6.38	620.55	1.50	620.90	0.32
z3		ET2535	0.669	0.2278	99.32%	46	0.13	2638	0.208	0.060151	0.182	0.818090	0.227	0.098685	0.114	0.607	608.05	3.94	606.98	1.04	606.70	0.66
z4		ET2535	0.707	0.0362	94.61%	6	0.17	335	0.220	0.059398	2.080	0.776350	2.205	0.094838	0.354	0.421	580.72	45.19	583.40	9.78	584.09	1.98
z5		ET2535	0.794	0.2433	99.35%	50	0.13	2789	0.247	0.060583	0.215	0.839405	0.266	0.100535	0.137	0.595	623.49	4.64	618.82	1.23	617.54	0.81
z6		ET2535	0.577	0.1827	98.92%	28	0.16	1678	0.179	0.060530	0.307	0.843389	0.353	0.101100	0.122	0.522	621.60	6.63	621.01	1.64	620.85	0.72

(a) z1, z2, *et cetera.* are labels for analyses composed of single zircon grains that were annealed and chemically abraded (Mattinson, 2005). Fragments from the same grain are denoted by z1a and z1b, z2a and z2b.

(b) Model Th/U ratio calculated from radiogenic $^{208}Pb/^{206}Pb$ ratio and $^{207}Pb/^{235}U$ date.

(c) Pb* and Pbc are radiogenic and common Pb, respectively. mol % $^{206}Pb^*$ is with respect to radiogenic and blank Pb.

(d) Measured ratio corrected for spike and fractionation only. For analyses that used the EARTHTIME ^{205}Pb-^{233}U-^{235}U tracer solution (ET535), Pb fractionation correction is 0.16 ± 0.03 (1 sigma) %/amu (atomic mass unit) based on recent analyses using EARTHTIME ^{202}Pb-^{205}Pb-^{233}U-^{235}U tracer solution (ET2535). For analyses that used the EARTHTIME ^{205}Pb-^{233}U-^{235}U tracer solution (ET535), Pb fractionation correction based on measurement of $^{202}Pb/^{205}Pb$ in the tracer solution.

(e) Corrected for fractionation and spike. Common Pb in zircon analyses is assigned to procedural blank with composition of $^{206}Pb/^{204}Pb$ = 18.04 ± 0.61%; $^{207}Pb/^{204}Pb$ = 15.54 ± 0.52%; $^{208}Pb/^{204}Pb$ = 37.69 ± 0.63% (1 sigma). $^{206}Pb/^{238}U$ and $^{207}Pb/^{206}Pb$ ratios corrected for initial disequilibrium in $^{230}Th/^{238}U$ using a D(Th/U) of 0.20 ± 0.05 (1 sigma). (f) Errors are 2 sigma, propagated using algorithms of Schmitz and Schoene (2007) and Crowley and others (2007).

(f) Errors are 2 sigma, propagated using algorithms of Schmitz and Schoene (2007) and Crowley and others (2007).

(g) Calculations based on the decay constants of Jaffey and others (1971) and $^{238}U/^{235}U$ of Hiess and others (2012). $^{206}Pb/^{238}U$ and $^{207}Pb/^{206}Pb$ dates corrected for initial disequilibrium in $^{230}Th/^{238}U$ using a D(Th/U) of 0.20 ± 0.05 (1 sigma).

*NAD27 CONUS datum.

TABLE 5

Summary of U-Pb dates and calculated errors

Sample number	Map Unit/location	$^{206}Pb/^{238}U$ date ± x / y /z * (Ma)	MSWD§/ (n)#
MT94-2C	Ash bed/Mystic Quarry, Somerville, MA	551.22 ± 0.20 / 0.33 / 0.66†	1.4/(7)
194-8A -210	Aplite sill/CTE Shaft 8	488.58 ± 0.16 / 0.29 / 0.58†	1.6/(5)
MTW2	Cambridge argillite/ BWT North Weymouth Shaft	598.74 ± 0.27 / 0.32 / 0.69†	1.8(2)
110 + 70	Cambridge argillite/IIT	597.78 ± 0.21 / 0.35 / 0.71	(1)
209 + 40	Cambridge argillite/BWT	584.09 ± 1.98 / 2.00 / 2.09	(1)

* All errors are 2σ and are expressed in two significant figures (details on U-Pb methods in Appendix). Where discussion in text requires random uncertainty only, the date itself is rounded to a single decimal place.

† Weighted mean $^{206}Pb/^{238}U$ date; other entries are analyses of single zircons.

§ Mean square of weighted deviates.

Number of analyses included in average (bold values in table 4).

Sample MT94-2C

This sample is from a 37 cm thick calcified ash bed in the Mystic River Quarry in Somerville, MA (figs. 2 and 3A). A concordant $^{207}Pb/^{206}Pb$ TIMS date of 568 Ma from a 6-grain, air abraded zircon fraction gave rise to the previously reported estimate of ~570 Ma as the age of this rock (Thompson and Bowring, 2000). An upper concordia intercept date of 639 ± 3 Ma from a linear array of six discordant multi-grain analyses revealed a component older zircon component as well. Results presented below were obtained from a magnetic split remaining from the earlier study. The zircon suite is dominated by prism fragments ranging from 50 to 150 μm. An average aspect ratio of 2.3 was determined from five unbroken prisms, and a few equant zircons <100 microns are also present.

Fifty-one single grains from sample MT94-2C (CL images in fig. A1.A, supplemental data) were analyzed by LA-ICPMS (Appendix table A1), and grains that yielded the nine youngest dates were analyzed with an additional spot. Two other grains that were not in the original group were also analyzed with two spots. For 10 of these 11 grains, the dates are equivalent (that is, probability of fit is >0.05). Weighted mean dates were calculated from these 10 grains, and these dates were used along with the single dates from grains in a relative probability plot (fig. 7A; n = 53). For the one grain with two spots that did not yield equivalent dates, the oldest date was used in the relative probability plot. The dominant peak in the plot is at 561 Ma, and there is a small peak at 638 Ma.

Seven grains from MT94-2C with young LA-ICPMS dates yielded CA-TIMS dates (table 4) that are equivalent with a weighted mean $^{206}Pb/^{238}U$ date of 551.22 ± 0.20/0.33/0.66 Ma (MSWD = 1.4, probability of fit = 0.20; concordia diagram in fig. 7A). The most conservative interpretation is that this date is the maximum depositional age of the ash. Because the dominant 561 Ma peak in the probability plot is within 2 percent of the CA-TIMS date and thus within resolution of the LA-ICPMS method, it is also reasonable to conclude that the majority of the zircon in the sample is likely the same age and that 551.22 ± 0.20 Ma (analytical uncertainty only) represents the depositional age of the ash. The 638 Ma peak in the relative probability plot reflects the presence of a minor xenocrystic or detrital zircon component.

Sample 194-8A −210

This sample is a piece of core boring from Shaft 8 of the City Tunnel Extension (figs. 2 and 3A). The rock represents a 1.2 m layer of sparsely porphyritic pink aplite containing 1 to 2 mm albite phenocrysts in a matrix of albite and quartz. Accessory

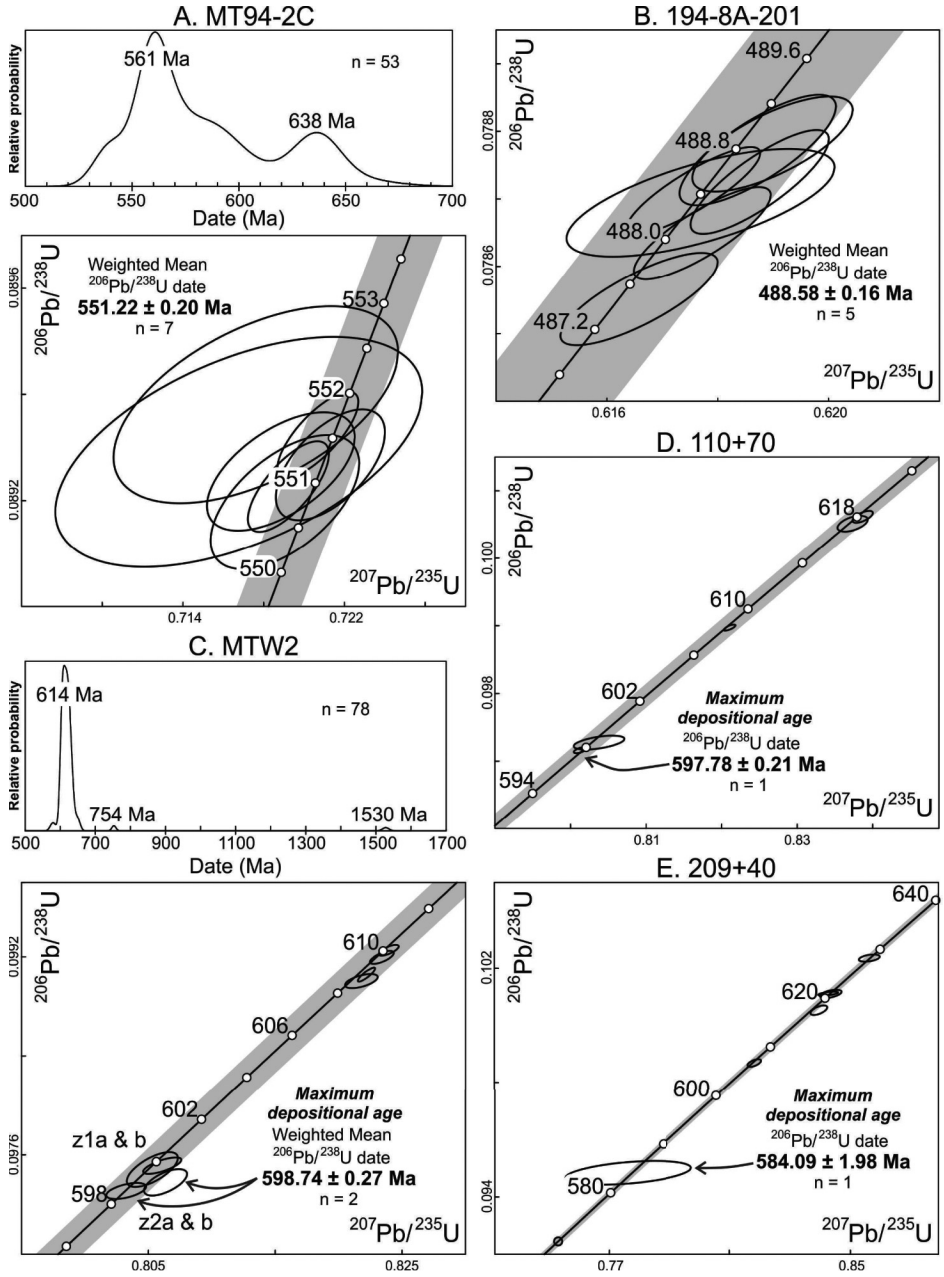

Fig. 7. Relative probability plots of LA-ICPMS U-Pb dates and concordia plots of CA-TIMS dates for samples from locations shown in figures 2 and 3. Concordia diagrams plotted with Isoplot 3.0 (Ludwig, 2003). Ages in Ma are marked on the concordia curve, and individual analyses of single zircons as shown as 2σ error ellipses. Gray areas behind concordias represent the decay constant uncertainties. Errors reported as ± x; complete U-Pb isotopic data and errors listed in tables 4 and 5, respectively. LA-ICPMS isotopic data in Appendix table A1. (A) Mystic Quarry ash bed, Somerville, MA. (B) Aplite sill intruding argillite, CTE Shaft 8A. (C) Argillite, BWT North Weymouth Shaft. (D) Argillite, IIT. (E). Argillite, BWT. CTE—City Tunnel Extension, BWT—Braintree Weymouth Tunnel, IIT—Inter-Island Tunnel.

minerals include apatite, monazite, pyrite and zircon showing oscillatory zoning in CL images (fig. A1.B, supplemental data). Five of seven zircons analyzed by CA-TIMS from this rock (table 4) are equivalent with a weighted mean of $^{206}Pb/^{238}U$ date of 488.58 ± 0.16/0.29/0.58 Ma (MSWD = 1.6, probability of fit = 0.18). Two other dates are 488.05 ± 0.33 and 487.47 ± 0.33 Ma (analytical uncertainty only). The weighted mean date is interpreted as the igneous crystallization age, and the two younger dates are interpreted as being from grains in which domains that suffered Pb loss were not completely removed by chemical abrasion (concordia diagram in fig. 7B).

The dated aplite resembles samples described as sills by M.P. Billings slightly to the north in the tunnel itself (unpublished notes in Harvard University Archives) and thus provides a minimum age for the argillite it intrudes.

Sample MTW2

This sample from the North Weymouth Shaft of the Braintree Weymouth Tunnel (figs. 2 and 3E) is coarse sandstone composed mainly of quartz, K-feldspar and lithic fragments including granite, myrmekite, volcanic rocks and a few quartzose sedimentary types (Q = 78.3 %, F = 4.5 %, L = 17.2 %). Detrital muscovite is bent around framework grains, and accessory apatite, monazite, sulfides and zircon are also present.

The strategy for this sample was to pick only euhedral zircon likely to yield the youngest dates. Selected grains ranging from 75 to 300 μm include some complete prisms with aspect ratios averaging ~2.5, oscillatory zoning and no cores, as well as numerous broken fragments of such grains (Appendix fig. A1.C). All but two of seventy-eight of these grains analyzed by LA-ICPMS yielded dates between 652 ± 12 and 576 ± 14 Ma (Appendix table A1), defining the principal peak on the probability density plot at 614 Ma (fig. 7C). Two grains of similar morphology yielded significantly older dates represented by probability peaks at 754 Ma and 1530 Ma (Appendix table A1). Six grains that yielded dates from the young end of the age spectrum were re-analyzed by CA-TIMS (concordia diagram in fig. 7C). Two of these were broken into two fragments that were analyzed separately. Two fragments from one grain (z1a,b in table 4) yield a weighted mean date of 599.78 ± 0.29/33/70 Ma (MSWD = 0.2, pof = 0.65) and two fragments from another grain (z2a,b in table 4) yield a weighted mean date of 598.74 ± 0.27/0.32/0.69 Ma (MSWD = 1.8, pof = 0.18). Four other dates are 610.03 ± 0.21 to 608.57 ± 0.27 Ma. The youngest date of 598.74 ± 0.27 (analytical error only) is interpreted as the maximum depositional age of the sandstone.

This result is consistent with a $^{207}Pb/^{206}Pb$ date of 599 Ma (reported without uncertainty by Green and others, 2002) for the youngest of several zircons from a siltstone higher in the North Weymouth shaft. All LA-ICPMS analyses overlap within uncertainty but CA-TIMS dates fall into two discreet age groups, both of which are consistent with sources in local granites listed in table 1 and discussed further in a later section.

Sample 110 + 70

This sample was collected in the Inter-Island Tunnel approximately 3.4 km south of the Deer Island Shaft (figs. 2 and 3D). The rock is laminated and contains ~40 modal percent angular fragments of quartz, plagioclase and chlorite-rich clots that may be altered volcanic rock fragments. These grains are studded through a felty matrix of muscovite + chlorite and accessory apatite, monazite, Fe-oxides and zircon. Extracted zircons were all sharply facetted, but sizes <50 μm were too small to mount for LA-ICPMS, so six of these were analyzed by CA-TIMS only (table 4). Five of these yielded dates from 618.00 ± 0.43 to 597.78 ± 0.21/0.35/0.71 Ma (analytical error only shown in fig. 7D). The youngest date is interpreted as the maximum depositional age.

Sample 209 + 40

This sample comes from the west wall of the Braintree Weymouth Tunnel approximately 0.4 km south of the Nut Island Shaft (figs. 2 and 3E). The sequence in this reach of the tunnel is well bedded on a scale of a few cm, and locally cross bedded. This particular sample shows a distinctly grainy texture, reflecting up to ~20 modal percent quartz and plagioclase crystals and more abundant phyllosilicate-rich clots, possibly altered lithic fragments. These grains are all silt-sized, and the inferred lithic fragments merge into a matrix of Fe-rich chlorite and illite. Millimeter-scale laminae are defined by horizons varying in grain size or crystal content. Secondary titanite and calcite are also present. Tiny, sharply facetted zircons in this sample were suitable only for CA-TIMS (table 4). Six grains from this sample yielded dates from 628.22 ± 0.59/2.00/2.09 to 584.09 ± 1.98/2.00/2.09 Ma (analytical error only in fig. 7E). The youngest date is interpreted as the maximum depositional age. The large uncertainty of this analysis reflects extremely low Pb in that zircon (z4 in table 4).

DISCUSSION

Structural Constraints on Stratigraphic Succession

Structural observations and interpretations bearing on regional stratigraphy of the Cambridge Formation are summarized below for each tunnel cross section in figure 3.

City Tunnel Extension.—Argillite in the top ~800 m of the ~2000 m CTE section is younger than the ~551 Ma Mystic Quarry ash bed (fig. 3A). Previous interpretations treating this sequence as a distal northerly facies of the Roxbury Conglomerate (Billings and Tierney, 1964; Billings, 1976) now dated at 595 to 584 Ma (M. Thompson and others, 2014) are no longer tenable. Relationships north of CTE Shaft 8 are better explained by a north-dipping normal fault along which younger Cambridge strata in the hanging wall were subsequently thrust back up over a rigid buttress of Roxbury Conglomerate in the footwall. Argillite beds north of the fault are sheared and locally transposed parallel to cleavage that is axial planar to a south-verging anticline (figs. 3A and 4D) developed during shortening accompanying the thrusting. The timing of this deformation is discussed in the Tectonics section.

North Metropolitan Relief Tunnel.—Micro-textures like those described above in the CTE are also found in samples RF22 and RF25 from shallow core borings south of Shaft 2 in the NMRT (fig. 3B). This zone is essentially on strike with, and thus interpreted as the eastward continuation of the reactivated normal fault in the CTE. South of the fault, the tunnel first transects the Charles River Syncline and then continues through north-dipping beds to Shaft 1 at Deer Island (fig. 2). The NMRT cross sections is quite generalized because of previously noted limitations on subsurface mapping. Billings (1975, p. 117) detailed various assumptions underlying "approximate" attitudes shown in his tunnel map, and many of these were judged too uncertain to incorporate into figure 2B. The need for structural steel in 24 percent of the tunnel further suggests the presence of undocumented faults. The estimated 2700 m thickness in the NMRT is best considered a maximum.

Main Drainage Tunnel.—The Cambridge Formation in the MDT begins east of Shaft B (fig. 3C) where 50 m of gray argillite sampled at borehole 195-12B overlies interbedded brownish, purplish and greenish argillite. The latter were assigned by Rahm (1962) to the Cambridge Formation, but are considered here to be coeval with Roxbury strata. Between here and Shaft C on the east, and assuming minor displacements on several normal faults, the tunnel transects a maximum of 1600 m of gray argillite that lies on the north limb of the Central Anticline (Billings, 1976; fig. 2).

Inter-Island Tunnel.—Approximately 545 m of section in the eastern end of the MDT continues southward across the Central Anticline and neighboring folds in the

IIT, and ~240 m more comprises the core of the Central Anticline (fig. 3D). Higher strata beginning at the level of sample 110 + 70 are younger than ~598 Ma and comprise ~1000 m of generally S-dipping gray argillite equivalent to NMRT horizons on the south limb of the Charles River Syncline. The argillite is more tightly folded north of a zone of more than 100 m of badly decomposed rock (Cathedral Fault of P. Thompson and others, 2014; fig. 3D) where Cambridge strata abut older, Roxbury-related brownish gray siltstone. This zone is interpreted here as another reactivated north-dipping normal fault. South of the fault zone, gently folded Cambridge strata overlying reddish argillite at the top of the Roxbury Conglomerate continue without discordance to the Nut Island Shaft where the IIT connects to the BWT (fig. 2).

Braintree-Weymouth Tunnel.—Cambridge strata south of Nut Island (fig. 2) are younger than ~584 Ma, the youngest detrital zircon obtained from sample 209 + 40 (fig. 3E). Here, in contrast to moderate dips and open folds in the IIT, gray argillite dips steeply south and is offset by high angle cross faults (fig. 2). North of Houghs Neck, argillite interbedded with muscovite-bearing quartzose sandstone is isoclinally folded and faulted against mafic volcanic rocks and related conglomerate shown on most maps as Roxbury Conglomerate (Zen, 1983, for example). This sequence is re-assigned here to the 597 to 593 Ma Lynn-Mattapan Volcanic Complex (Zlmv, Zlmn in figs. 2, 3E and 3F) because conglomerate clast assemblages here lack quartzite lithotypes ubiquitous in Roxbury deposits (M. Thompson and others, 2014). Normal faulting followed by thrust reactivation is necessary to explain isoclinal folds in younger argillite in the hanging wall of this fault.

The top of the south-dipping Houghs Neck assemblage is sheared, and overlying argillite shows increasingly strong cleavage, along with overturned and transposed bedding (fig. 4E) and multiple thrust faults. There is much gray argillite in the deformed sequence, but also greenish and reddish horizons, as well as quartzose sandstone (Q in fig. 3E) including sample MTW2 which yields a maximum depositional age of ~599 Ma. These data together with the presence of a trilobite fragment in a thin section of red shale near the south end of the tunnel (lower Cambrian Weymouth Formation of Landing, 1988) suggest that the Cambridge Formation in this area spans the Ediacaran-Cambrian boundary. The sandstone-bearing sequence is distinguished as a separate, transitional member of the Cambridge Formation (stippled Zct in fig. 3E). Quartzose sandstone associated with Cambridge argillite in surface outcrops around Quincy, MA (beneath legend in fig. 2) was called Milton quartzite by Billings (1982).

Stratigraphic thickness in the BWT can only be stated within broad limits due to structural complexities described above. Minimum thickness for the lower part of the section is 1300 m, including ~90 m of synclinally folded gray argillite north of the Nut Island Shaft (fig. 3D) and ~1200 m of uncleaved argillite to the south (fig. 3E). The transitional sequence south of Houghs Neck (Zct in fig. 3E) is realistically much thinner than the transected thickness of ~2150 m shown in figure 8. However, quantifying the effects of thrust duplication and repetitions related to transposed bedding is not possible.

Dorchester Tunnel—Steeply south-dipping argillite starting slightly north of Shaft 7C (fig. 3F) is much disrupted by faults of indeterminable throw according to Richardson (1977). He reported a thickness of 4000 feet (~1200 m), which is in reasonable agreement with ~1100 m measured in figure 3E constructed using his structural measurements. Fault relations between the Cambridge Formation and the Lynn-Mattapan Volcanic Complex resemble those in the BWT, but these faults do not connect along strike (fig. 2).

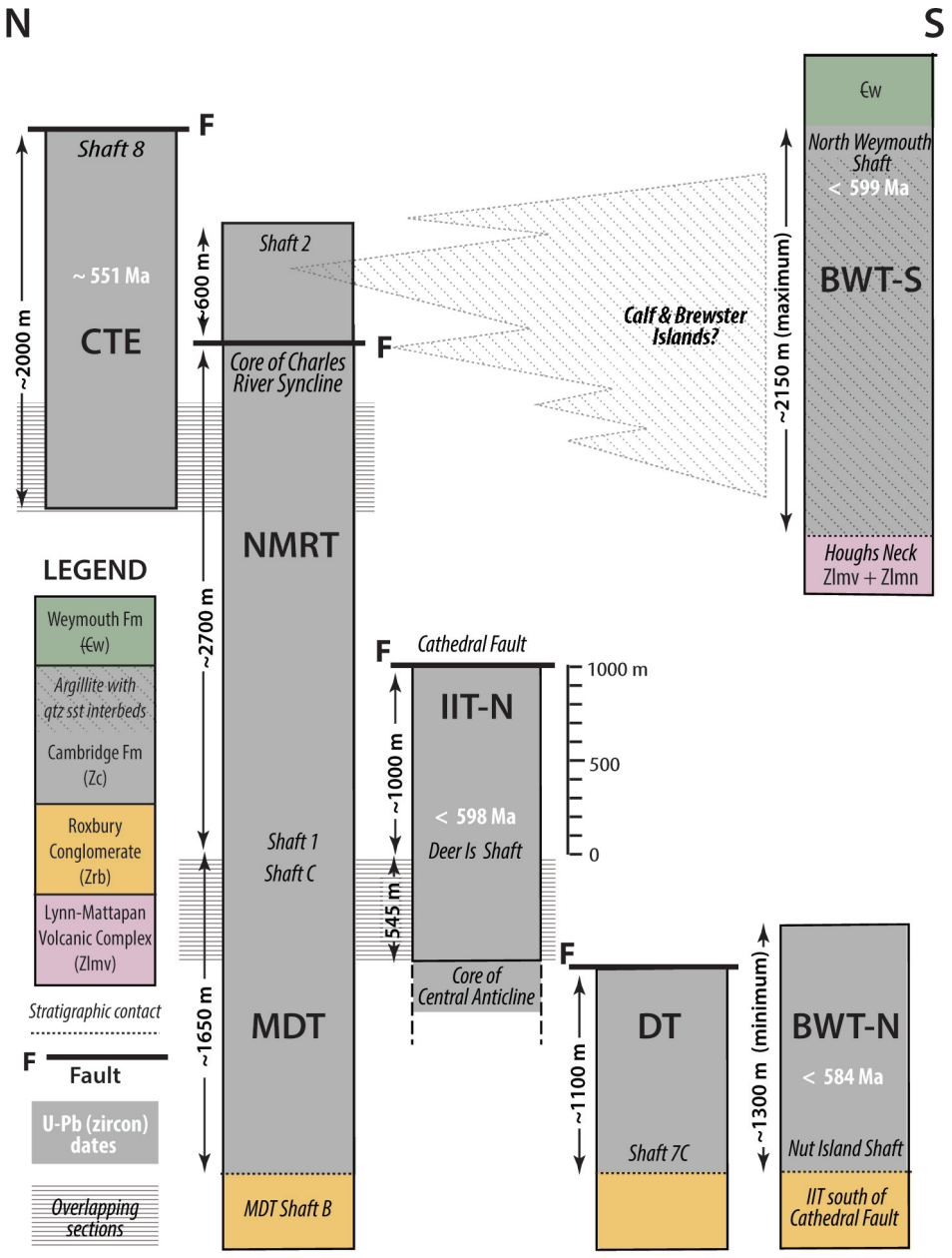

Fig. 8. Regional stratigraphy of the Cambridge Formation inferred from structural relationships in Boston-area tunnels and available U-Pb zircon geochronology. The approximate stratigraphic position of argillites on Calf, Middle Brewster and Outer Brewster islands is based on the estimate of P. Thompson and others (2014), but no thickness was indicated. CTE—City Tunnel Extension, NMRT—North Metropolitan Relief Tunnel, MDT—Main Drainage Tunnel, IIT—Inter-Island Tunnel, DT—Dorchester Tunnel, BWT—Braintree Weymouth Tunnel.

Stratigraphic Synthesis

Individual tunnel sections are integrated in figure 8 as columns showing thicknesses estimated above from cross sections in figure 3. The datum for this construction

is the Roxbury-Cambridge contact transected in several of the tunnels, and the columns are arranged from north to south across the map area (fig. 2).

The most continuous sequence above the datum is found in the MDT and NMRT that connect at Deer Island (fig. 2). This section totaling ~4350 m is cut off by the fault south of NMRT Shaft 2 (fig. 3B). Argillite thicknesses of ~1000 m in the IIT-N, and ~1100 m in the DT (fig. 8) correspond to middle and lower horizons of the composite MDT-NMRT column.

Younger parts of the Cambridge Formation border the northern and southern margins of the Boston Basin. The youngest units in the north lie above the ~551 Ma Mystic Quarry ash bed in the ~2000 m CTE section (fig. 3A). This portion of the sequence is inferred to have been originally higher than the top of the NMRT column because of its position in the hanging wall of the reactivated normal fault that extends from the CTE into the NMRT (figs. 2, 3A, and 3B). The hanging wall section in the NMRT (above fault in fig. 8) contains quartzose sandstone with trace amounts of detrital muscovite, thus permitting a link with similar interbeds in the BWT-S. Here, the interbedded sandstone-argillite with a maximum estimated thickness of ~2150 m (stippled Zct in fig. 3E) passes without obvious break into trilobite-bearing strata of the lower Cambrian Weymouth Formation. At least some of this apparent Ediacaran-Cambrian transitional sequence must be younger than ~551 Ma, though major faults through the central part of the Basin preclude linking the CTE and the BWT-S directly. The positions shown in figure 8 are consistent with observed ages.

The integrated thickness of the Cambridge Formation in the northern Boston Basin is ~5350 m assuming that CTE and MDT-NMRT sections overlap as shown in figure 8. This total is in unexpectedly good agreement with the ~5700 m estimate of Billings (1975 and 1976) given the revised interpretations outlined above in each of the tunnels. Requiring the Cambrian segment of the BWT-S section to be younger than the ~551 Mystic Quarry ash bed does not add to the regional thickness, and placing it in this position allows a proximal-distal relationship between argillites and associated quartzose sandstone interbeds with more northerly Cambridge units. Turbiditic Cambridge strata on Calf and the Brewster islands (fig. 1) lie at an estimated elevation of ~4500 m above the top of the Roxbury Conglomerate (P. Thompson and others, 2014), and these too may also be part of the proximal assemblage. The facies relationship in figure 8 is slightly modified from Billings' (1976) depositional model for the Basin in that it excludes the 595 to 584 Ma Roxbury Conglomerate. Reassignment of conglomerate at Houghs Neck to the 597 to 593 Ma Lynn-Mattapan Volcanic Complex (M. Thompson and others, 2014; Zlmn in figs. 2 and 8) means also that the Cambridge Formation in this area rests on a regional angular unconformity.

Cambridge deposition as determined from BWT-N sample 209 + 40 (fig. 3E) began after 584.09 ± 1.98 Ma, the same age as sills (Zb in fig. 2) that establish the minimum age of the Roxbury Conglomerate (M. Thompson and others, 2014). The 551.22 ± 0.20 Ma minimum age near the top of the northern argillite (fig. 3A) implies a depositional interval of >30 Ma. This interval exceeds 40 Ma if the BWT-S section spans the Ediacaran-Cambrian boundary. An alternative possibility of a post-Roxbury depositional hiatus will be discussed in the section on Cross-terrane Linkages.

Detrital Zircon Provenance

Detrital zircon selection from tunnel samples 110 + 70, 209 + 40 and MTW2 (fig. 2) concentrated on sharply facetted zircon euhedra likely to yield the youngest possible maximum depositional age for the Cambridge Formation. The number of analyses was further limited because only MTW2 contained zircon large enough for LA-ICPMS. However, seventeen high precision CA-TIMS $^{206}Pb/^{238}U$ dates from all three samples (table 4) were sufficient to establish a ~584 Ma maximum age reflecting detritus from underlying Roxbury Conglomerate and to provide a number of other

insights on argillite provenance. Discussion below also incorporates earlier TIMS analyses of five air abraded zircons from an argillite in the CTE (<2% discordant $^{207}Pb/^{206}Pb$ dates from sample 198-14 of Thompson and Bowring, 2000).

All twenty-two TIMS dates fall within the 614 Ma probability peak established by 76 of 78 LA-ICPMS analyses from sample MTW2 (fig. 7C). Apart from the ~584 Ma zircon highlighted above, all of these dates also correspond to published crystallization ages for pre-Roxbury Ediacaran granitoids and volcanic rocks in greater Boston and across SE New England (dates and sources in table 1). At least part of the Dedham Granite was already exposed during the main phase of arc-related magmatism in southeastern New England because ~597 Ma Lynn-Mattapan volcanic rocks and related conglomerate rest unconformably on 609 Ma Dedham Granite in Hingham, MA (fig. 1; Thompson and others, 2010). Transpressional faulting in conjunction with oblique subduction in the model of Nance and others (2008) could provide a mechanism for the necessary uplift. Dedham emplacement at ~10 km—the middle of the 2-4kb pressure range estimated by Dillon (ms, 1994)—implies an exhumation rate of 0.8 mm/yr, comparable to values derived from low-temperature thermochronometry along many parts of the transpressional San Andreas fault system (for example, Spotila and others, 2007; Moser and others, 2017). Continued unroofing to expose younger plutons (table 1) is consistent with ages of detrital zircons in 595 to 584 Ma Roxbury Conglomerate (M. Thompson and others, 2014).

The six youngest detrital zircons (~599–596 Ma) were obtained from samples MTW2, 110 + 70 and 198-14, and these are consistent with crystallization ages of Lynn-Mattapan volcanic rocks and/or from slightly older Westwood, Cohasset and Esmond granites. The largest group, comprising eight ~610 to 603 Ma dates from the four tunnel samples, fall within the documented age range of the Dedham Granite and Dedham Granite North of Boston. Uncertainties on the youngest two analyses in this group allow overlaps with slightly younger Milford and Fall River granites, and larger uncertainties on granitoid gneisses associated with the Milford Granite permit additional matches. A single ~612 Ma zircon from the CTE fits only with the Northbridge gneiss, and six older dates between ~628 and 618 Ma are nominally consistent with the first reported crystallization ages of the Esmond Granite (Hermes and Zartman, 1985) or Hope Valley Alaskite (Zartman and others, 1988), but these are likely to be too old because batch zircon samples of that era were not pre-treated to minimize Pb loss. In short, all of the tunnel samples contain detritus consistent with derivation from local bedrock sources. East-northeast-trending groove casts and slump folds overturned to the east in the MDT imply deposition on east facing slopes (Rahm, 1962) and suggest possible Dedham and Milford granite sources (undifferentiated in fig. 1) located in the vicinity of Milford, Massachusetts.

The 551.22 ± 0.20 Ma Mystic Quarry ash bed yielded a bimodal LA-ICPMs age spectrum (fig. 7A) with an older, subordinate peak at 638 Ma. Eighteen zircons contributing to this peak are interpreted as xenocrystic components in the eruption cloud or reworked detrital components from underlying argillite. None of the grains contributing to this peak was re- analyzed via CA-TIMS, but $^{207}Pb/^{206}Pb$ dates of ~637 and ~635 Ma were previously obtained from multi-grain zircon fractions in the same sample (z46, z47 *in* Thompson and Bowring, 2000). These dates and 628 to 618 Ma dates discussed above might signal the presence of hitherto unrecognized pre-Dedham magmatic units in southeastern New England, but as discussed below, sources in other West Avalonian terranes are also possible.

Cross-terrane Linkages

The Cambridge Formation has commonly been compared with similarly thick and monotonously gray sequences comprising the Conception Group in Newfoundland's Avalon Peninsula (Thompson and Bowring, 2000; Nance and others, 2008, for

example; inset map in fig. 1). Instead, U-Pb zircon age constraints presented here imply potential correlation with younger sequences in West Avalonian lithostratigraphic columns shown in figure 9.

The most promising source for the ~551 Ma volcanic ash near the top of the Cambridge Formation is found in the >8 km thick Coldbrook Group of New Brunswick's Caledonia terrane (Giles and Rutenberg, 1977; Barr and White, 1999 and 2004; fig. 1 inset and fig. 9). Volcanic rocks in this sequence include flows of basaltic, andesitic and rhyolitic composition, along with intermediate to felsic lapilli tuff, crystal tuff and volcanic breccia that are interpreted as largely subaerial in origin. Interbedded with the pyroclastic units are tuffaceous conglomerate and laminated tuffaceous siltstone.

Early U-Pb dating of the Coldbrook assemblage (mostly $^{207}Pb/^{206}Pb$ dates on multi-grain, air-abraded zircon fractions of Bevier and Barr, 1990; Barr and others, 1994; Miller and others, 2000) has lately been augmented by single crystal $^{206}Pb/^{238}U$ dates obtained via LA-ICPMS (Barr and others, 2018 and references therein). Among the latter are crystallization ages of 552.8 ± 1.6 Ma and 553.3 ± 3 Ma for rhyolitic units in the bimodal upper Coldbrook Group exposed in coastal portions of the southern Caledonia Highlands. These, together with a date of 557.4 ± 2.5 Ma from dacite in the lower Coldbrook Group located farther inland, constrain Coldbrook volcanism between 560 and 550 Ma (fig. 9). The Mystic Quarry ash bed lies near the end of this interval, and thus could represent airborne tephra that travelled far from subaerial Coldbrook eruption sites to be deposited along with fine-grained siliclastic marine sediment (figs. 4A, 4B, and 4C) in the Cambridge Formation of the northern Boston Basin.

Detrital muscovite in quartzite samples like MTW2 at the top of the Cambridge Formation (figs. 3E and 8) suggest linkage with latest Ediacaran to lowest Cambrian deposits recording the onset of stable platform conditions across West Avalonia. Of particular interest are quartzite interbeds described in the Ratcliffe Brook Formation (Barr and others, 2003; Reynolds and others, 2009; fig. 9) that overlies Coldbrook volcanic rocks in the Caledonia terrane. Siltstone near the top of the Ratcliffe Brook Formation is also micaceous. In the broader view of Landing (1996, 2004), these units are respectively treated as equivalents of the Rencontre Formation and Chapel Island Formation in southeastern Newfoundland. The overlying Random Formation in Newfoundland (Hiscott, 1982) is represented in the Caledonia and Mira terranes by the Glen Falls Formation (Tanoli and Pickerell, 1988) and Sgadan Lake Formation (Barr and others, 1996), both of which include quartzites containing detrital muscovite. Depositional settings for these units vary from fluvial to marginal and open marine, and gray or greenish gray Cambridge argillite in the BWT is consistent with the latter category. Beyond representing similar sedimentary facies, all these deposits seem likely to share some yet-to-be recognized source for their muscovite components.

Other possible links with the Caledonia section are suggested by >610 Ma detrital zircons in Cambridge samples. Source rocks of such ages have yet to be recognized in southeastern New England, but are found in volcanic rocks and cross-cutting plutons comprising the 630 to 615 Ma Broad River Group in southern New Brunswick (Bevier and Barr, 1990; Barr and White, 1999). Ages in this range along with some as old as ~640 Ma are also reported in the Cobequid highlands of northern mainland Nova Scotia (Murphy and others, 1997; White and others, 2019 and 2020), providing potential sources for inherited zircon contributing to the 638 Ma probability peak in the Mystic Quarry ash sample.

Other similarities also suggest closer relationships between southeastern New England, New Brunswick and northern mainland Nova Scotia than with more northerly Avalonian terranes in Cape Breton island and Newfoundland. Among the few possible "peri-Gondwanan basement" occurrences throughout West Avalonia (Hibbard and others, 2006) are quartzites in the Westboro Formation (fig. 1) that yielded a

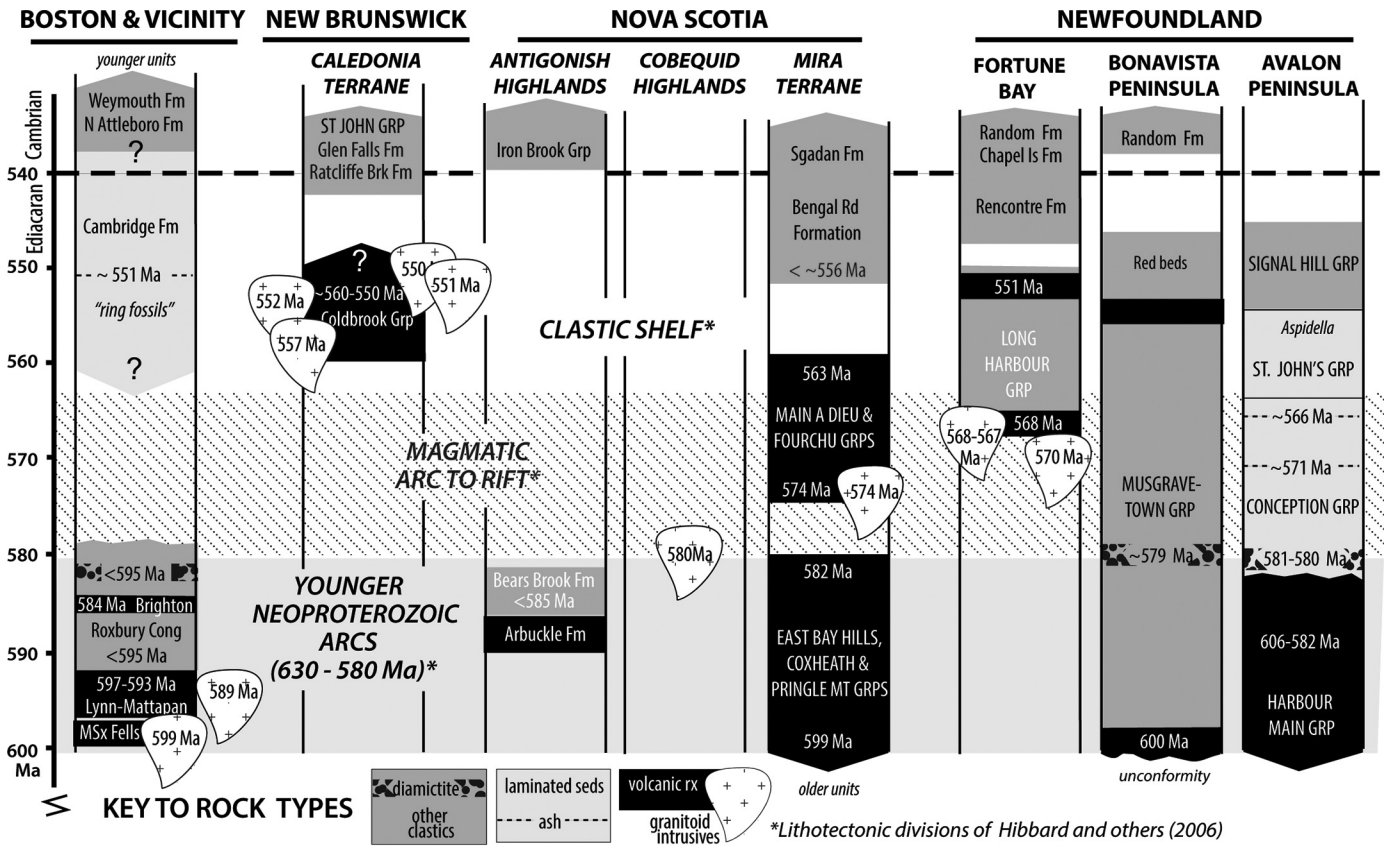

Fig. 9. Tectono-stratigraphic comparison between upper Ediacaran through Cambrian sequences in the Boston-area sector of Avalonia in southeastern New England and more northerly "West" Avalonian terranes of New Brunswick, Nova Scotia and Newfoundland, Canada. Date sources: Boston and vicinity—Hampton (2017), Thompson and others (1996, 2007, 2014 and this study), Caledonia terrane—Barr and White (1999 and 2004), Barr and others (1994 and 2018), Miller and others (2000), Antigonish and Cobequid highlands—Pe-Piper and Piper (2002), White and others (2019), Mira terrane—Bevier and others (1993), Wilner and others (2013). Newfoundland—Krogh and others (1988), O'Brien and others (1996), Mills and others (2016), Pu and others (2016).

detrital zircon spectrum and <912 Ma maximum age similar to those documented in samples from the Gamble Brook Formation in the Cobequid Highlands (Thompson and others, 2012; White and others, 2020). Main-phase Avalonian plutonism in southeastern New England (610–590 Ma in table 1) corresponds most closely in age to bodies in the Antigonish and Cobequid highlands (Thompson and others 2010). Low negative ϵ_{Nd} values for SE New England granitoids likewise more resemble Cobequid and Antigonish values than high positive values indicative of juvenile sources for Newfoundland and Mira terrane granitoids (Thompson and others, 2012). The presence of significant gaps in the geologic record above Ediacaran arc complexes in New Brunswick and mainland Nova Scotia (fig. 9) makes this a plausible possibility in southeastern New England as well.

The interpretation shown in figure 9 is consistent with "elliptical markings" originally described by Clark (1923, p. 483) in Hingham, Massachusetts (fig. 1) as resembling *Aspidella terranovica* Billings, 1872 in Precambrian rocks known now as the St. John's Group (fig. 9) which lies above the Conception Group with its ~566 Ma ash bed at Mistaken Point (CA-TIMS $^{206}Pb/^{238}U$ date of Pu and others, 2016; fig. 9). The small size of the Hingham structures led Clark to conclude that they are inorganic features rather than *Aspidella*, but later workers have likened them to discoidal forms of comparable age in the Longmyndian Supergroup of southern England and Wales (Bailey and Bland, 2001; 566.1 ± 3.1 and 559.3 ± 1.9 Ma SHRIMP U-Pb dates of Compston and others, 2002; further discussion in Noble and others, 2015). In either case, deposition of pre-551 Ma portions of the Cambridge Formation can reasonably be inferred as starting after ~566 Ma.

Tectonic Setting

The Cambridge Formation falls between Ediacaran subduction-related magmatic and sedimentary rocks in southeastern New England and Cambrian strata recording stable shelf conditions in this area. Age constraints presented above place Cambridge deposition within the intervening transition interval marked by the development of extensional basins reflecting oblique collision and ultimately ridge-trench collision (Nance and Murphy, 1996: Nance and others, 2002, 2008). As illustrated by the tectono-stratigraphic columns in figure 9, the transitional rock record is highly variable both within and among West Avalonian terranes.

The arc-to-platform transition in southeastern New England most resembles relationships in the Caledonia terrane of New Brunswick. Magmatic arc sequences in both places are followed by a significant hiatus before renewed activity starting around 560 Ma (fig. 9). In New Brunswick this took the form of voluminous Coldbrook volcanism accompanying rifting of the 630 to 615 Ma Broad River Group (Barr and White, 1999). Around Boston, Cambridge deposition overspread an erosion surface variously exposing 595 to 584 Roxbury Conglomerate and 597 to 593 Ma Lynn-Mattapan volcanic rocks at the top of the arc complex. The contrasting regimes in New Brunswick and southeastern New England are linked through the 551 Ma Mystic Quarry ash bed near the top of the Cambridge Formation and volcanic ash components throughout the thick argillite section. Multiple normal faults documented in Boston-area tunnels (fig. 3) suggest that Cambridge sedimentation also took place in conjunction with rifting. Extension was already in progress during Roxbury deposition and led to localized depocenters in which Roxbury-related sandstones accumulated distinct detrital zircon populations (Thompson and others, 2014). Continuing or renewed normal faulting during Cambridge time quite likely elevated previously upfaulted blocks even further, thereby accentuating topographic irregularities of the sub-Cambridge unconformity. The NE to ENE strikes of these faults are consistent with sinistral transcurrent motions envisioned in the transform model of Nance and others (2008). The protracted fault history also reinforces the interpretation linking signifi-

cantly depleted del$^{18}O_{WR}$ values in Ediacaran granites and volcanic rocks across southeastern New England with meteoric-hydrothermal fluid circulation driven by extensional basin formation (Potter and others, 2008).

Thrust reactivation is necessary to explain asymmetric, south-verging folds with steep axial planar cleavage in hanging wall blocks of the CTE and IIT (figs. 3A and 3D). Steep south dips, and in the extreme, overturned beds in the BWT (fig. 3E) find counterparts in Pennsylvanian rocks overthrust by Dedham Granite on the north margin of the Norfolk Basin (Chute, 1966; Volckmann, 1967) located southwest of figure 2. The simplest explanation for this similarity is that all of these structures formed during the Alleghanian collision between Gondwana and previously accreted Avalonia on the eastern margin of Laurentia (340–330 Ma in van Staal and Barr, 2012).

CONCLUSIONS

Regional structure and stratigraphy, composition, age and Avalonian tectonic significance of the poorly exposed argillaceous Cambridge Formation are reinterpreted here using subsurface data from water supply and sewerage tunnels beneath the Boston Basin and Boston Harbor to the east. These jointly provide a continuous transect starting with the City Tunnel Extension and the North Metropolitan Relief Tunnel on the north and proceeding though the Main Drainage Tunnel, the Dorchester Tunnel, the Inter-Island Tunnel and the Braintree Weymouth Tunnel on the south.

Argillaceous sedimentary rocks dominate the >5 km composite stratigraphic section integrating thicknesses determined from individual tunnel cross sections. Whole-rock major element and REE compositions of tunnel samples and related core borings reveal a sedimentary mixture of terrigenous and volcanic components deposited in a deep marine basin. This sequence rests variously on magmatic-arc-related units of the 595 to 584 Ma Roxbury Conglomerate (MDT and IIT) or 597 to 593 Ma Lynn-Mattapan Volcanic Complex (southern BWT), implying a regional sub-Cambridge unconformity. Deposition started after ~584 Ma, the youngest CA-TIMS date from detrital zircon in argillite approximately 500 m above Roxbury Conglomerate in the Inter-Island Tunnel. Combined LA-ICPMS and CA-TIMS dates establish a depositional age of ~551 Ma from an ash bed sampled in surface exposure near the top of the Cambridge section in Somerville, MA. The Cambridge sequence ends in argillite interbedded with muscovite-bearing quartzose sandstone in southern reaches of the Braintree Weymouth Tunnel. This sequence passes without obvious break into trilobite-bearing strata of the lower Cambrian Weymouth Formation, nominally suggesting a depositional interval exceeding 40 Ma. The interpretation preferred here is that Cambridge strata were deposited after an ~20 Ma hiatus above a significant regional unconformity.

Cambridge deposition, whenever it started, occurred during the interval of wrench faulting and bimodal magmatism that succeeded the Avalonian magmatic arc after about 570 Ma in "West" Avalonian terranes extending from southeastern New England through Atlantic Canada to the Avalon Peninsula, Newfoundland. Evidence for the post-arc transtensional regime is found throughout the Boston-area tunnel network in the form of normal faults with hanging wall blocks of Cambridge strata down-dropped against Roxbury or Lynn-Mattapan units. The ~551 Ma Mystic Quarry ash bed and ash admixed throughout the Cambridge section reflect contemporaneous though distant magmatic activity. Proposed sources for this material are voluminous ~560 to 550 Ma eruptions recorded in the Coldbrook Group of New Brunswick's Caldonia terrane. Latest Ediacaran to Cambrian deposits above the Coldbrook Group include micaceous quartzite analogous to interbeds in the Cambridge Formation below Cambrian units in the Braintree Weymouth Tunnel. Likely counterparts for pre-551 Ma Cambridge horizons include argillaceous units in the <566 Ma St. John's Group, Newfoundland.

Ediacaran normal faulting was followed by thrust reactivation to produce asymmetric, south-verging folds with steep N-dipping axial planar cleavages in the hanging wall blocks. Deformation intensifies on the south margin of the Boston Basin as evidenced by steep to over-turned and transposed beds in the Braintree Weymouth Tunnel. These structures may reflect Alleghanian orogenesis.

ACKNOWLEDGMENTS

This study would not have been possible without the efforts of past and present Massachusetts Water Resources Authority personnel including John Kaplin, Bill Levy, Mary Lydon, and John Nelson who made available records and core borings both from pre-1960 Boston-area tunnels and from renewed tunneling beginning after the 1986 federal court order to clean up Boston Harbor. Most remarkably, visits were permitted to the Inter-Island Tunnel in 1995 and to the Braintree Weymouth Tunnel in 2000 and 2001. Geologist Thom Davidson guided our activities in the BWT and later shared his invaluable mapping logs prepared for Stone & Webster, Inc. Analysis of tunnel-related materials began via independent study projects by Wellesley College geology majors Rachel Friedman, Tracy Johnston Zager, Theresa Green and Kristin Morell. Whole rock geochemistry and U-Pb zircon geochronology were initially supported by National Science Foundation Grants EAR96-28520 and EAR-0001134 (to Thompson), and lately by Brachman Hoffman Small Grants from Wellesley College. Thanks also to Nelson Eby for REE analyses of representative argillite samples, to Robert Jacobi for insights on fault structures, to Claire McKinley and Rachel Scudder for perspectives on sedimentary geochemistry, to Greg Dunning for recalculating the Cohasset Granite date in table 1, and to Raquel Alonso Perez for access to the Billings Collection at Harvard University. This paper has benefited from reviews by Sandra Barr, Chris Hepburn and Brendan Murphy.

APPENDIX

U-Pb geochronology methods at Boise State University Isotope Geology Laboratory LA-ICPMS methods.—Zircon grains separated from samples using standard techniques were annealed at 900 °C for 60 hours in a muffle furnace, and mounted in epoxy and polished until their centers were exposed. Cathodoluminescence [CL] images were obtained with a JEOL JSM-1300 scanning electron microscope and Gatan MiniCL. Zircon was analyzed by laser ablation inductively coupled plasma mass spectrometry [LA-ICPMS] using a ThermoElectron X-Series II quadrupole ICPMS and New Wave Research UP-213 Nd:YAG UV (213 nm) laser ablation system. In-house analytical protocols, standard materials, and data reduction software were used for acquisition and calibration of U-Pb dates and a suite of high field strength elements [HFSE] and rare earth elements [REE]. Zircon was ablated with a laser spot of 25 μm wide using fluence and pulse rates of 5 J/cm^2 and 10 Hz, respectively, during a 45 second analysis (15 sec gas blank, 30 sec ablation) that excavated a pit ~25 μm deep. Ablated material was carried by a 1.2 L/min He gas stream to the nebulizer flow of the plasma. Dwell times were 5 ms for Si and Zr, 200 ms for ^{49}Ti and ^{207}Pb, 80 ms for ^{206}Pb, 40 ms for ^{202}Hg, ^{204}Pb, ^{208}Pb, ^{232}Th, and ^{238}U and 10 ms for all other HFSE and REE. Background count rates for each analyte were obtained prior to each spot analysis and subtracted from the raw count rate for each analyte. Ablations pits that appear to have intersected glass or mineral inclusions were identified based on Ti and P. U-Pb dates from these analyses are considered valid if the U-Pb ratios appear to have been unaffected by the inclusions. Analyses that appear contaminated by common Pb were rejected based on mass 204 being above baseline. For concentration calculations, background-subtracted count rates for each analyte were internally normalized to ^{29}Si and calibrated with respect to NIST SRM-610 and −612 glasses as the primary standards. Temperature was calculated from the Ti-in-zircon thermometer (Watson

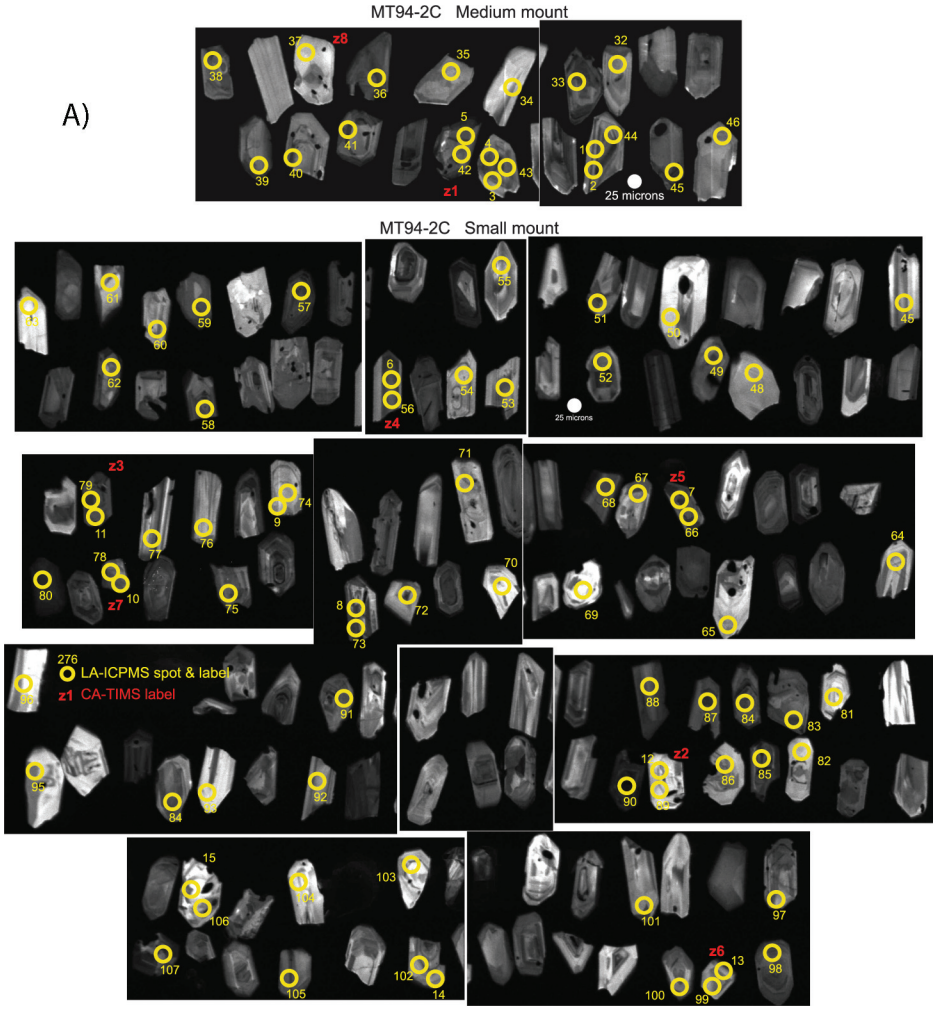

Fig. A1. CL images of zircon with LA-ICPMS spot locations and analysis labels in red and CA-TIMS analysis labels in yellow. For each sample, there are separate mounts showing small (S), medium (M) and in one case large (L) grains. CL contrast and brightness can be compared within a mount and sample, but not between mounts or samples. (A) Sample MT92-4C. (B) Sample 194-8A −210. (C) Sample MTW2.

and others, 2006). Because there are no constraints on the activity of TiO_2, an average value in crustal rocks of 0.8 was used.

Data for MT94-2C were collected in two experiments in March 2018 (Appendix table A1). For MTW2, data were collected in one experiment in March 2019 (Appendix table A1). For U-Pb and $^{207}Pb/^{206}Pb$ dates, in both cases, instrumental fractionation of the background-subtracted ratios was corrected and dates were calibrated with respect to interspersed measurements of zircon standards and reference materials. The primary standard Plešovice zircon (Sláma and others, 2008) was used to monitor time-dependent instrumental fractionation based on two analyses for every 10 analyses of unknown zircon. A secondary correction to the $^{206}Pb/^{238}U$ dates was made based on results from the zircon standards Seiland (530 Ma, unpublished data, Boise State University) and Zirconia (327 Ma, unpublished data, Boise State University), which

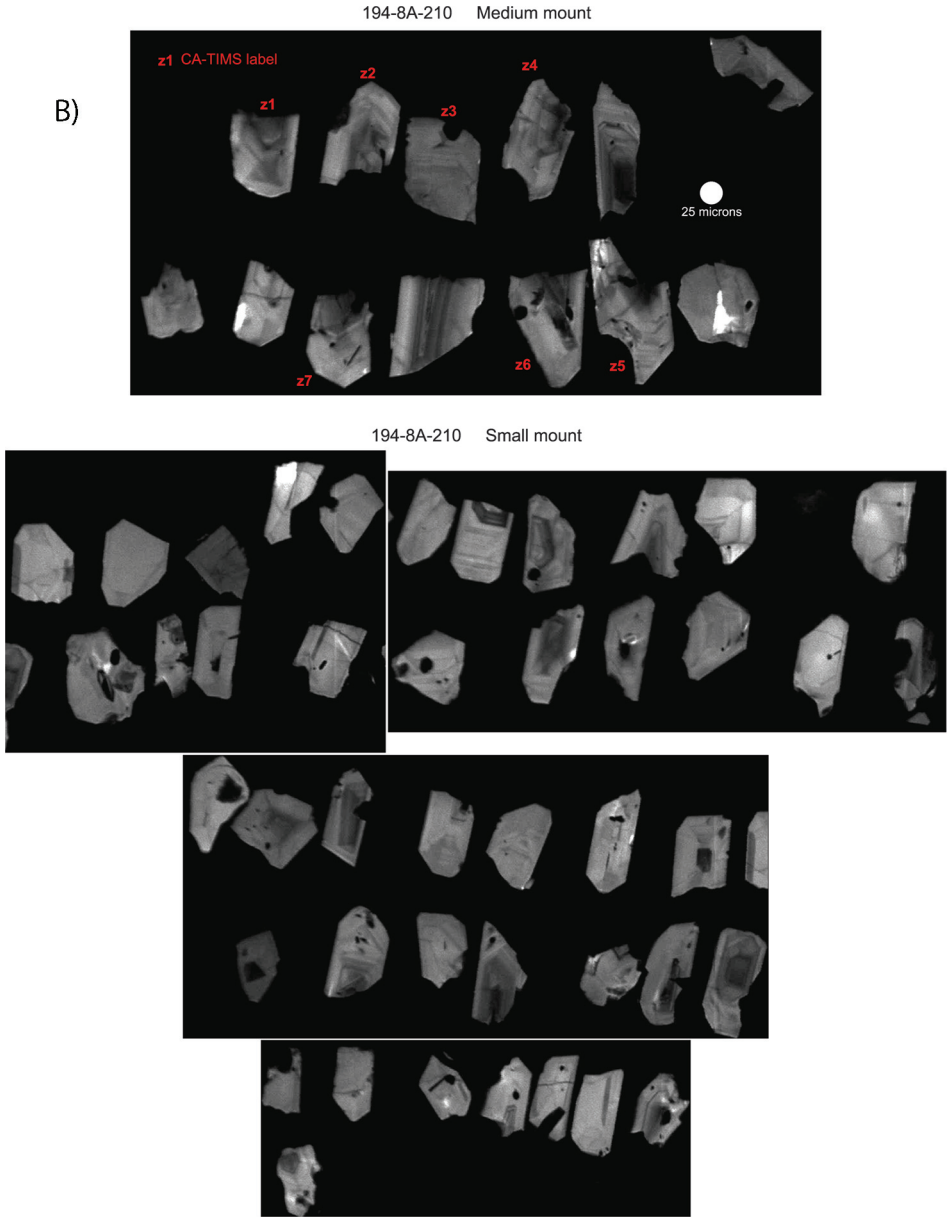

Fig. A1. (continued)

were treated as unknowns and measured once for every 10 analyses of unknown zircon. These results showed a linear age bias of several percent that is related to the ^{206}Pb count rate. The secondary correction is thought to mitigate matrix-dependent variations due to contrasting compositions and ablation characteristics between the Plešovice zircon and other standards (and unknowns).

Radiogenic isotope ratio and age error propagation for all analyses includes uncertainty contributions from counting statistics and background subtraction.

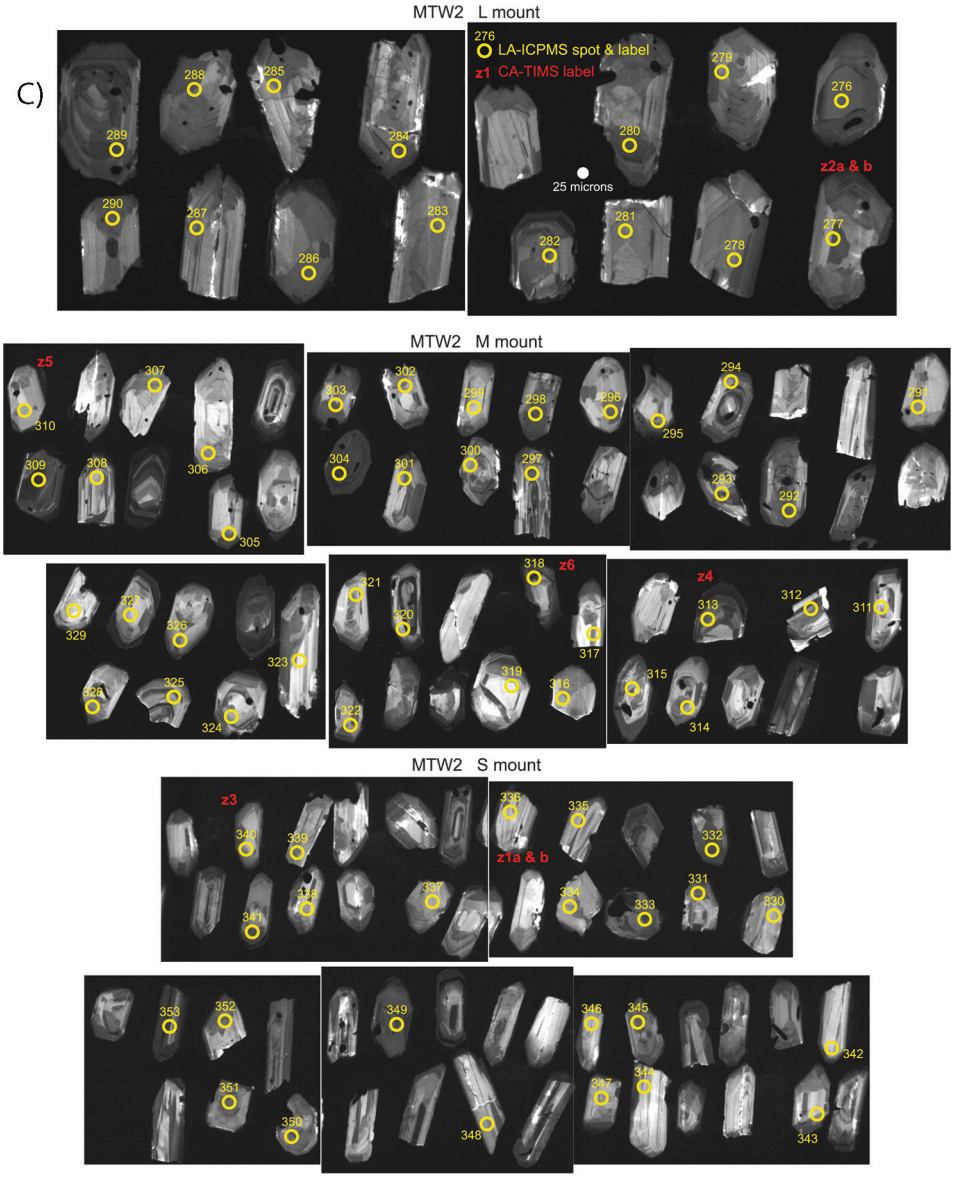

Fig. A1. (continued)

Weighted mean dates are calculated using Isoplot 3.0 (Ludwig, 2003). The standard calibration uncertainty is the local standard deviation of the polynomial fit to the interspersed primary standard measurements versus time for the time-dependent, $^{206}Pb/^{238}U$ fractionation factor. This uncertainty is 1.4% (2σ) for both [March 2018] experiments. Age interpretations are based on $^{206}Pb/^{238}U$ dates. Errors on the dates are at 2σ.

CA-TIMS U-Pb geochronology methods.—Zircon grains separated from samples using standard techniques were annealed at 900 °C for 60 hours in a muffle furnace.

TABLE A1

LA-ICPMS isotopic data

		Corrected isotope ratios							Dates (Ma) †						
Analysis	CA-TIMS label	207Pb*/235U*	±2σ (%)	206Pb*/238U	±2σ (%)	error corr.	207Pb*/206Pb*	±2σ (%)	207Pb*/206Pb*	±2σ (Ma)	207Pb*/235U	±2σ (Ma)	206Pb*/238U*	±2σ (Ma)	% disc.
MT94-2C: Mystic Quarry ash bed, Somerville, MA (UTM coordinates: 19T 03 27 667 E, 46 95 589 N) §															
MT94-2C 31		0.73986	6.21	0.09282	3.46	0.55	0.05781	5.15	523	113	562	27	**572**	19	-9
MT94-2C 31		0.84057	5.98	0.10077	3.91	0.64	0.06050	4.53	621	98	619	28	**619**	23	0
MT94-2C 31		0.72256	###	0.09245	3.83	0.32	0.05669	11.27	479	249	552	51	**570**	21	-19
MT94-2C 31	z8	0.73837	###	0.09079	3.68	0.3	0.05898	11.53	566	251	561	52	**560**	20	1
MT94-2C 31		0.90338	4.58	0.10375	3.31	0.71	0.06315	3.16	713	67	654	22	**636**	20	11
MT94-2C 31		0.98474	6.51	0.11896	3.78	0.57	0.06004	5.30	605	115	696	33	**725**	26	-20
MT94-2C 31		0.78049	9.25	0.09362	3.79	0.4	0.06047	8.44	620	182	586	41	**577**	21	7
MT94-2C 31		0.82134	6.22	0.09593	3.07	0.48	0.06210	5.41	678	116	609	28	**590**	17	13
MT94-2C 31	z1	0.70544	4.85	0.08397	2.50	0.5	0.06093	4.15	637	89	542	20	**520**	12	18
MT94-2C 3		0.73344	5.45	0.08938	3.30	0.59	0.05952	4.34	586	94	559	23	**552**	17	6
MT94-2C 4		0.77082	5.78	0.09381	3.26	0.55	0.05959	4.77	589	103	580	26	**578**	18	2
MT94-2C 1		0.72087	6.38	0.09175	2.91	0.44	0.05698	5.68	491	125	551	27	**566**	16	-15
MT94-2C 2		0.69870	8.35	0.08935	3.51	0.41	0.05671	7.58	480	167	538	35	**552**	19	-15
													560	12	Weighted mean date
MT94-2C 45		0.76297	6.70	0.09325	3.64	0.54	0.05934	5.62	580	122	576	29	**575**	20	1
MT94-2C 47		0.82309	5.61	0.09888	2.96	0.51	0.06037	4.77	617	103	610	26	**608**	17	1
MT94-2C 49		0.91995	6.38	0.10759	3.68	0.57	0.06202	5.21	675	112	662	31	**659**	23	2
MT94-2C 51		0.85472	5.04	0.10073	3.25	0.63	0.06154	3.84	658	82	627	24	**619**	19	6
MT94-2C 53		0.82721	6.96	0.09880	3.62	0.51	0.06072	5.95	629	128	612	32	**607**	21	3
MT94-2C 56	z4	0.78477	###	0.08746	3.40	0.3	0.06508	10.71	777	225	588	50	**541**	777	30
MT94-2C 6	z4	0.77272	###	0.08930	4.44	0.38	0.06276	10.59	700	226	581	51	**551**	700	21
													554	14	Weighted mean date
MT94-2C 58		0.84743	5.74	0.10199	3.81	0.65	0.06026	4.29	613	93	623	27	**626**	23	-2
MT94-2C 59		0.85382	7.21	0.10307	3.49	0.48	0.06008	6.30	606	136	627	34	**632**	21	-4
MT94-2C 60		0.75788	6.91	0.09344	3.64	0.52	0.05883	5.88	561	128	573	30	**576**	20	-3
MT94-2C 62		0.81423	7.75	0.09976	4.15	0.53	0.05919	6.54	574	142	605	35	**613**	24	-7
MT94-2C 64		0.79802	5.98	0.09418	2.73	0.44	0.06146	5.33	655	114	596	27	**580**	15	11
MT94-2C 65		0.75145	9.91	0.09149	5.05	0.5	0.05957	8.53	588	185	569	43	**564**	27	4
MT94-2C 66	z5	0.71999	5.33	0.08636	2.87	0.52	0.06047	4.50	620	97	551	23	**534**	15	14
MT94-2C 7	z5	0.79720	6.72	0.08972	2.68	0.38	0.06444	6.16	756	130	595	30	**554**	14	27
													544	10	Weighted mean date

TABLE A1

(continued)

Analysis	CA-TIMS label	Corrected isotope ratios: 207Pb*/235U*	±2σ (%)	206Pb*/238U	±2σ (%)	error corr.	207Pb*/206Pb*	±2σ (%)	Dates (Ma) †: 207Pb*/206Pb*	±2σ (Ma)	207Pb*/235U	±2σ (Ma)	206Pb*/238U*	±2σ (Ma)	% disc.
MT94-2C: Mystic Quarry ash bed, Somerville, MA (UTM coordinates: 19T 03 27 667 E, 46 95 589 N) §															
MT94-2C 68		0.84545	5.98	0.09976	5.14	0.85	0.06147	3.07	656	66	622	28	**613**	30	7
MT94-2C 70		0.69811	7.48	0.09108	3.65	0.48	0.05559	6.53	436	145	538	31	**562**	20	-29
MT94-2C 71		0.75463	8.92	0.09174	4.52	0.5	0.05966	7.69	591	167	571	39	**566**	24	4
MT94-2C 73		0.72038	4.64	0.08934	4.06	0.86	0.05848	2.24	548	49	551	20	**552**	21	-1
MT94-2C 8		0.90174	###	0.09190	1.99	0.18	0.07116	10.03	962	205	653	49	**567**	11	41
													564	10	Weighted mean date
MT94-2C 74		0.75099	8.32	0.08927	4.50	0.54	0.06101	7.00	640	151	569	36	**551**	24	14
MT94-2C 9		0.77234	###	0.09365	4.21	0.34	0.05981	11.32	597	245	581	53	**577**	23	3
													564	17	Weighted mean date
MT94-2C 3		0.73344	5.45	0.08938	3.30	0.59	0.05952	4.34	586	94	559	23	**552**	17	6
MT94-2C 4		0.77082	5.78	0.09381	3.26	0.55	0.05959	4.77	589	103	580	26	**578**	18	2
MT94-2C 1		0.72087	6.38	0.09175	2.91	0.44	0.05698	5.68	491	125	551	27	**566**	16	-15
MT94-2C 2		0.69870	8.35	0.08935	3.51	0.41	0.05671	7.58	480	167	538	35	**552**	19	-15
													560	12	Weighted mean date
MT94-2C 75		0.84014	6.89	0.10249	2.46	0.34	0.05945	6.44	584	140	619	32	**629**	15	-8
MT94-2C 78	z7	0.71491	4.90	0.08848	3.34	0.67	0.05860	3.59	552	78	548	21	**547**	17	1
MT94-2C 10	z7	0.73541	6.96	0.09079	2.76	0.38	0.05875	6.39	558	139	560	30	**560**	15	0
													554	11	Weighted mean date
MT94-2C 79	z3	0.71525	4.58	0.08736	3.00	0.64	0.05938	3.46	581	75	548	19	**540**	16	7
MT94-2C 80		0.80980	5.34	0.09810	3.93	0.73	0.05987	3.61	599	78	602	24	**603**	23	-1
MT94-2C 81		0.68966	###	0.09334	4.93	0.41	0.05358	10.72	354	242	533	49	**575**	27	-63
MT94-2C 82		0.75978	8.47	0.09301	5.12	0.6	0.05924	6.74	576	147	574	37	**573**	28	0
MT94-2C 83		0.67936	9.61	0.09219	4.92	0.51	0.05345	8.26	348	187	526	39	**568**	27	-63
MT94-2C 84		0.83714	7.64	0.10218	4.41	0.57	0.05942	6.24	582	135	618	35	**627**	26	-8
MT94-2C 85		0.81918	5.73	0.10380	3.27	0.56	0.05724	4.71	501	104	608	26	**637**	20	-27
MT94-2C 88		0.71567	4.03	0.09100	2.92	0.71	0.05704	2.78	493	61	548	17	**561**	16	-14
MT94-2C 89		0.72530	7.66	0.08746	3.80	0.49	0.06015	6.64	609	144	554	33	**540**	20	11
MT94-2C 12		0.69700	7.76	0.08683	4.62	0.59	0.05822	6.23	538	136	537	32	**537**	24	0
													539	15	Weighted mean date
MT94-2C 92		0.71888	7.57	0.09108	3.35	0.44	0.05724	6.78	501	149	550	32	**562**	18	-12
MT94-2C 93		0.74567	9.44	0.09594	4.84	0.51	0.05637	8.10	467	179	566	41	**591**	27	-27

TABLE A1
(continued)

Analysis	CA-TIMS label	Corrected isotope ratios: 207Pb*/235U*	±2σ (%)	206Pb*/238U	±2σ (%)	error corr.	207Pb*/206Pb*	±2σ (%)	Dates (Ma) †: 207Pb*/206Pb*	±2σ (Ma)	207Pb*/235U	±2σ (Ma)	206Pb*/238U*	±2σ (Ma)	% disc.
MT94-2C: Mystic Quarry ash bed, Somerville, MA (UTM coordinates: 19T 03 27 667 E, 46 95 589 N) §															
MT94-2C 95		0.72732	###	0.09307	4.98	0.41	0.05668	11.02	479	244	555	52	**574**	27	-20
MT94-2C 97		0.75592	7.64	0.09589	4.04	0.52	0.05717	6.48	498	143	572	33	**590**	23	-18
MT94-2C 99	z6	0.71896	6.67	0.08984	2.78	0.41	0.05804	6.06	531	133	550	28	**555**	15	-4
MT94-2C 13	z6	0.75639	6.66	0.09001	4.01	0.59	0.06095	5.32	637	115	572	29	**556**	21	13
													555	12	Weighted mean date
MT94-2C 100		0.86788	9.45	0.10451	3.22	0.33	0.06023	8.88	612	192	634	45	**641**	20	-5
MT94-2C 102		0.72645	7.45	0.08946	3.34	0.44	0.05890	6.66	563	145	554	32	**552**	18	2
MT94-2C 14		0.89515	###	0.09216	2.98	0.28	0.07044	9.93	941	203	649	50	**568**	16	40
													561	12	Weighted mean date
MT94-2C 103		0.80037	###	0.09552	4.01	0.34	0.06077	11.01	631	237	597	53	**588**	23	7
MT94-2C 104		0.72585	8.13	0.09131	3.37	0.41	0.05765	7.39	517	162	554	35	**563**	18	-9
MT94-2C 105		0.91732	7.78	0.10634	5.79	0.74	0.06256	5.19	693	111	661	38	**651**	36	6
MT94-2C 106		0.71313	8.69	0.08958	3.63	0.41	0.05774	7.89	520	173	547	37	**553**	19	-6
MT94-2C 15		0.78540	8.46	0.09165	3.11	0.36	0.06215	7.87	679	168	589	38	**565**	17	17
													560	13	Weighted mean date
MT94-2C 107		0.88963	6.10	0.10310	3.74	0.6	0.06258	4.82	694	103	646	29	**633**	23	9
MT94-2C 109		0.69422	###	0.09068	3.95	0.38	0.05553	9.47	433	211	535	43	**560**	21	-29

Notes for Sample MT94-2C analyses:
Experiment on March 13, 2018 in black
Isotope ratio and date errors include systematic calibration errors of 0.64% (207Pb/206Pb) and 1.40% (206Pb/238U) (2 sigma).
Trace element concentrations were deleted from analyses known to have intersected inclusions of other minerals based on P and Ti.
Ablation used a laser spot size of 25 microns and a laser firing repetition rate of 10 Hz.
Activity of TiO_2 for Ti-in-Zircon temperature calculation is 0.8.
Experiment on March 15, 2018 in red
Isotope ratio and date errors include systematic calibration errors of 0.76% (207Pb/206Pb) and 1.42% (206Pb/238U) (2 sigma).
Trace element concentrations were deleted from analyses known to have intersected inclusions of other minerals based on P and Ti.
Ablation used a laser spot size of 25 microns and a laser firing repetition rate of 10 Hz.
Activity of TiO_2 for Ti-in-Zircon temperature calculation is 0.8.
† **Best date in bold type.**
§ NAD27 CONUS datum

TABLE A1
(continued)

Analysis	CA-TIMS label	Corrected isotope ratios 207Pb*/235U*	±2σ (%)	206Pb*/238U	±2σ (%)	error corr.	207Pb*/206Pb*	±2σ (%)	Dates (Ma) † 207Pb*/206Pb*	±2σ (Ma)	207Pb*/235U	±2σ (Ma)	206Pb*/238U*	±2σ (Ma)	% disc.
MTW2: Micaceous quartzose sandstone, BWT North Weymouth Shaft (UTM coordinates: 19T 03 38 005 E, 46 78 742 N*) §															
MTW2 L 276		3.49319	2.54	0.26671	2.34	0.91	0.09499	1.01	**1528**	19	1526	20	1524	32	0
MTW2 M 304		1.04162	2.59	0.12391	1.68	0.64	0.06097	1.97	638	42	725	13	**753**	12	-18
MTW2 S 353		0.86487	3.07	0.10639	1.98	0.64	0.05896	2.34	566	51	633	14	**652**	12	-15
MTW2 S 349		0.86470	3.50	0.10612	2.53	0.72	0.05910	2.42	571	53	633	16	**650**	16	-14
MTW2 S 332		0.87819	3.80	0.10532	2.04	0.53	0.06047	3.21	621	69	640	18	**646**	13	-4
MTW2 S 334		0.92932	4.07	0.10360	1.61	0.39	0.06506	3.74	776	79	667	20	**635**	10	18
MTW2 S 348		0.87373	3.42	0.10357	1.89	0.54	0.06118	2.85	646	61	638	16	**635**	11	2
MTW2 M 315		0.86953	3.81	0.10334	2.09	0.54	0.06103	3.18	640	68	635	18	**634**	13	1
MTW2 M 322		0.83284	4.44	0.10300	2.87	0.64	0.05864	3.38	554	74	615	20	**632**	17	-14
MTW2 M 309		0.82345	3.54	0.10290	2.60	0.73	0.05804	2.40	531	53	610	16	**631**	16	-19
MTW2 M 325		0.85648	3.30	0.10266	1.88	0.56	0.06051	2.72	622	59	628	15	**630**	11	-1
MTW2 L 286		0.85248	3.32	0.10264	2.45	0.73	0.06024	2.24	612	48	626	16	**630**	15	-3
MTW2 S 343		0.86543	4.18	0.10237	2.26	0.53	0.06131	3.52	650	76	633	20	**628**	14	3
MTW2 S 351		0.83029	3.99	0.10222	2.57	0.64	0.05891	3.05	564	66	614	18	**627**	15	-11
MTW2 S 330		0.83383	7.04	0.10222	4.03	0.57	0.05916	5.77	573	126	616	33	**627**	24	-9
MTW2 S 338		0.85129	3.31	0.10211	2.03	0.61	0.06047	2.61	620	56	625	15	**627**	12	-1
MTW2 M 293		0.86036	3.42	0.10210	1.81	0.52	0.06112	2.91	643	62	630	16	**627**	11	3
MTW2 M 324		0.81431	3.73	0.10209	2.14	0.57	0.05785	3.06	524	67	605	17	**627**	13	-20
MTW2 L 283		0.86482	5.36	0.10208	2.29	0.42	0.06144	4.85	655	104	633	25	**627**	14	4
MTW2 L 280		0.86278	4.49	0.10206	2.15	0.47	0.06131	3.94	650	85	632	21	**626**	13	4
MTW2 M 301		0.82038	3.83	0.10192	2.01	0.52	0.05838	3.26	544	71	608	18	**626**	12	-15
MTW2 M 311		0.80409	4.51	0.10162	2.09	0.46	0.05739	4.00	507	88	599	20	**624**	12	-23
MTW2 L 288		0.84437	5.27	0.10155	2.72	0.51	0.06030	4.51	615	97	622	24	**623**	16	-1
MTW2 M 299		0.98114	3.91	0.10152	2.09	0.53	0.07009	3.30	931	68	694	20	**623**	12	33
MTW2 S 352		0.79734	4.74	0.10148	2.29	0.48	0.05698	4.15	491	92	595	21	**623**	14	-27
MTW2 M 327		0.84574	3.75	0.10144	2.07	0.54	0.06047	3.13	620	67	622	17	**623**	12	0
MTW2 M 306		0.84246	4.90	0.10132	2.33	0.47	0.06031	4.31	615	93	620	23	**622**	14	-1
MTW2 M 305		0.82353	4.54	0.10130	2.14	0.47	0.05896	4.00	566	87	610	21	**622**	13	-10
MTW2 M 294		0.82237	3.98	0.10126	2.13	0.53	0.05890	3.36	563	73	609	18	**622**	13	-10
MTW2 M 317		0.79437	4.99	0.10114	1.99	0.39	0.05696	4.57	490	101	594	22	**621**	12	-27
MTW2 M 298		0.83378	3.79	0.10113	2.10	0.55	0.05980	3.15	596	68	616	17	**621**	12	-4
MTW2 M 326		0.84361	4.08	0.10111	2.66	0.65	0.06051	3.09	622	67	621	19	**621**	16	0
MTW2 L 278		0.84521	4.56	0.10104	2.32	0.50	0.06067	3.92	627	84	622	21	**621**	14	1
MTW2 S 337		0.83252	4.52	0.10088	2.89	0.64	0.05985	3.47	598	75	615	21	**620**	17	-4

TABLE A1
(continued)

Analysis	CA-TIMS label	Corrected isotope ratios: 207Pb*/235U*	±2σ (%)	206Pb*/238U	±2σ (%)	error corr.	207Pb*/206Pb*	±2σ (%)	Dates (Ma) †: 207Pb*/206Pb*	±2σ (Ma)	207Pb*/235U	±2σ (Ma)	206Pb*/238U*	±2σ (Ma)	% disc.
MTW2: Micaceous quartzose sandstone, BWT North Weymouth Shaft (UTM coordinates: 19T 03 38 005 E, 46 78 742 N*) §															
MTW2 L 290		0.86652	4.06	0.10078	2.19	0.53	0.06236	3.43	687	73	634	19	**619**	13	10
MTW2 M 292		0.85091	3.56	0.10074	2.50	0.70	0.06126	2.53	648	54	625	17	**619**	15	5
MTW2 M 329		0.81975	3.49	0.10053	1.84	0.52	0.05914	2.97	572	65	608	16	**618**	11	-8
MTW2 S 345		0.82605	3.97	0.10050	2.33	0.58	0.05961	3.21	590	70	611	18	**617**	14	-5
MTW2 M 312		0.84116	4.40	0.10048	2.96	0.67	0.06071	3.26	629	70	620	20	**617**	17	2
MTW2 M 319		0.83535	4.47	0.10044	2.42	0.54	0.06032	3.76	615	81	617	21	**617**	14	0
MTW2 L 284		0.85118	3.61	0.10033	2.49	0.68	0.06153	2.61	658	56	625	17	**616**	15	6
MTW2 L 279		0.83130	4.75	0.10033	2.81	0.59	0.06009	3.83	607	83	614	22	**616**	17	-2
MTW2 M 328		0.81435	3.83	0.10033	1.63	0.42	0.05887	3.47	562	76	605	17	**616**	10	-10
MTW2 S 344		0.82810	4.19	0.10005	2.41	0.57	0.06003	3.43	605	74	613	19	**615**	14	-2
MTW2 S 350		0.79945	3.26	0.10000	2.02	0.61	0.05798	2.56	529	56	597	15	**614**	12	-16
MTW2 M 302		0.82763	3.98	0.09995	2.81	0.70	0.06005	2.83	606	61	612	18	**614**	16	-1
MTW2 M 297		0.81675	3.24	0.09988	1.78	0.54	0.05931	2.70	578	59	606	15	**614**	10	-6
MTW2 S 331		0.80774	4.38	0.09978	1.99	0.45	0.05871	3.90	556	85	601	20	**613**	12	-10
MTW2 S 342		0.80009	3.48	0.09953	1.68	0.47	0.05830	3.04	541	67	597	16	**612**	10	-13
MTW2 L 289		0.83326	3.27	0.09945	2.90	0.88	0.06077	1.52	631	33	615	15	**611**	17	3
MTW2 M 308		0.82440	3.52	0.09945	2.46	0.69	0.06012	2.53	608	55	611	16	**611**	14	-1
MTW2 L 285		0.80036	4.21	0.09945	1.73	0.40	0.05837	3.84	544	84	597	19	**611**	10	-12
MTW2 M 321		0.84697	3.62	0.09944	2.00	0.55	0.06178	3.01	666	64	623	17	**611**	12	8
MTW2 M 296		0.81828	4.19	0.09930	2.77	0.66	0.05977	3.14	595	68	607	19	**610**	16	-3
MTW2 L 287		0.79894	5.46	0.09921	2.05	0.37	0.05841	5.07	545	111	596	25	**610**	12	-12
MTW2 M 316		0.82899	5.24	0.09906	2.20	0.42	0.06069	4.75	628	102	613	24	**609**	13	3
MTW2 M 303		0.82241	4.33	0.09903	2.12	0.48	0.06023	3.78	612	82	609	20	**609**	12	1
MTW2 M 291		0.80786	4.81	0.09888	2.72	0.56	0.05926	3.97	577	86	601	22	**608**	16	-5
MTW2 L 281		0.80182	5.40	0.09888	2.48	0.45	0.05882	4.80	560	105	598	24	**608**	14	-8
MTW2 S 333		0.81642	3.18	0.09887	1.93	0.60	0.05989	2.52	599	55	606	15	**608**	11	-1
MTW2 M 300		0.80269	3.64	0.09881	1.85	0.50	0.05892	3.13	564	68	598	16	**607**	11	-8
MTW2 M 307		0.85037	3.93	0.09876	2.98	0.75	0.06245	2.57	689	55	625	18	**607**	17	12
MTW2 M 320		0.84116	2.28	0.09872	1.56	0.67	0.06180	1.66	667	36	620	11	**607**	9	9
MTW2 S 335		0.80646	3.45	0.09871	1.72	0.49	0.05926	2.99	577	65	600	16	**607**	10	-5
MTW2 M 295		0.82958	3.94	0.09868	1.62	0.40	0.06097	3.59	638	77	613	18	**607**	9	5
MTW2 S 341		0.79937	2.43	0.09856	1.42	0.57	0.05882	1.97	561	43	596	11	**606**	8	-8
MTW2 S 347		0.81563	3.78	0.09854	1.92	0.50	0.06003	3.26	605	71	606	17	**606**	11	0
MTW2 M 314		0.79245	4.32	0.09852	2.49	0.57	0.05834	3.53	542	77	593	19	**606**	14	-12

TABLE A1
(continued)

Analysis	CA-TIMS label	Corrected isotope ratios: 207Pb*/235U*	±2σ (%)	206Pb*/238U	±2σ (%)	error corr.	207Pb*/206Pb*	±2σ (%)	Dates (Ma) †: 207Pb*/206Pb*	±2σ (Ma)	207Pb*/235U	±2σ (Ma)	206Pb*/238U*	±2σ (Ma)	% disc.
MTW2: Micaceous quartzose sandstone, BWT North Weymouth Shaft (UTM coordinates: 19T 03 38 005 E, 46 78 742 N*) §															
MTW2 S 339		0.80260	3.89	0.09838	1.76	0.44	0.05917	3.47	573	75	598	18	**605**	10	-5
MTW2 M 318	z6	0.79787	2.41	0.09824	1.55	0.63	0.05890	1.85	563	40	596	11	**604**	9	-7
MTW2 M 310	z5	0.76607	4.36	0.09818	1.72	0.39	0.05659	4.01	476	89	578	19	**604**	10	-27
MTW2 S 346		0.79257	3.41	0.09808	1.67	0.48	0.05860	2.97	552	65	593	15	**603**	10	-9
MTW2 M 323		0.81216	4.71	0.09785	1.45	0.30	0.06020	4.48	611	97	604	21	**602**	8	1
MTW2 M 313	z4	0.80193	3.00	0.09778	2.35	0.78	0.05948	1.86	585	40	598	14	**601**	14	-3
MTW2 S 340	z3	0.79879	3.23	0.09724	1.53	0.46	0.05958	2.84	588	62	596	15	**598**	9	-2
MTW2 L 277	z2a+ b	0.77557	4.37	0.09454	2.32	0.52	0.05950	3.71	585	80	583	19	**582**	13	1
MTW2 S 336	z1a+b	0.78727	3.01	0.09342	2.50	0.82	0.06112	1.69	644	36	590	13	**576**	14	11

Notes for Sample MTW2 analyses:
Experiment on March 22, 2019
Isotope ratio and date errors do not include systematic calibration errors of 0.34% ($^{207}Pb/^{206}Pb$) and 0.58% ($^{206}Pb/^{238}U$) (2 sigma).
Trace element concentrations were deleted from analyses known to have intersected inclusions of other minerals based on P and Ti.
Ablation used a laser spot size of 25 microns and a laser firing repetition rate of 10 Hz.
Activity of TiO2 for Ti-in-Zircon temperature calculation is 0.8.
L—zircon in large mount, M—zircon in medium mount, S—zircon in small mount (fig. 7C)
† Bold type indicates best age.

Cathodoluminescence [CL] images were obtained using a JEOL JSM-1300 scanning electron microscope and Gatan MiniCL. U-Pb dates were obtained by the chemical abrasion isotope dilution thermal ionization mass spectrometry [CA-TIMS] method from analyses composed of single zircon grains (table 4), modified after Mattinson (2005).

Zircon was put into 3 ml Teflon PFA beakers and loaded into 300 μl Teflon PFA microcapsules. Fifteen microcapsules were placed in a large-capacity Parr vessel and the zircon partially dissolved in 120 μl of 29 M HF for 12 hours at 190 °C. Zircon was returned to 3 ml Teflon PFA beakers, HF was removed, and zircon was immersed in 3.5 M HNO_3, ultrasonically cleaned for an hour, and fluxed on a hotplate at 80 °C for an hour. The HNO_3 was removed and zircon was rinsed twice in ultrapure H_2O before being reloaded into the 300 μl Teflon PFA microcapsules (rinsed and fluxed in 6 M HCl during sonication and washing of the zircon) and spiked with the EARTHTIME mixed ^{233}U-^{235}U-^{205}Pb tracer solution. Zircon was dissolved in Parr vessels in 120 μl of 29 M HF with a trace of 3.5 M HNO_3 at 220 °C for 48 hours, dried to fluorides, and re-dissolved in 6 M HCl at 180 °C overnight. U and Pb were separated from the zircon matrix using an HCl-based anion-exchange chromatographic procedure (Krogh, 1973), eluted together and dried with 2 μl of 0.05 N H_3PO_4.

Pb and U were loaded on a single outgassed Re filament in 5 μl of a silica-gel/phosphoric acid mixture (Gerstenberger and Haase, 1997), and U and Pb isotopic measurements made on a GV Isoprobe-T multicollector thermal ionization mass spectrometer equipped with an ion-counting Daly detector. Pb isotopes were measured by peak-jumping all isotopes on the Daly detector for 160 cycles, and corrected for 0.16 ± 0.03%/a.m.u. (1 sigma error) mass fractionation. Transitory isobaric interferences due to high-molecular weight organics, particularly on ^{204}Pb and ^{207}Pb, disappeared within approximately 30 cycles, while ionization efficiency averaged 10^4 cps/pg of each Pb isotope. Linearity (to $\geq 1.4 \times 10^6$ cps) and the associated deadtime correction of the Daly detector were determined by analysis of NBS982. Uranium was analyzed as UO_2^+ ions in static Faraday mode on 10^{12} ohm resistors for 300 cycles, and corrected for isobaric interference of $^{233}U^{18}O^{16}O$ on $^{235}U^{16}O^{16}O$ with an $^{18}O/^{16}O$ of 0.00206. Ionization efficiency averaged 20 mV/ng of each U isotope. U mass fractionation was corrected using the known $^{233}U/^{235}U$ ratio of the EARTHTIME tracer solution.

CA-TIMS U-Pb dates and uncertainties were calculated using the algorithms of Schmitz and Schoene (2007), EARTHTIME ET535 tracer solution (Condon and others, 2015) with calibration of $^{235}U/^{205}Pb = 100.233$, $^{233}U/^{235}U = 0.99506$, and $^{205}Pb/^{204}Pb = 11268$, and U decay constants recommended by Jaffey and others (1971). $^{206}Pb/^{238}U$ ratios and dates were corrected for initial ^{230}Th disequilibrium using $D_{Th/U} = 0.20 \pm 0.05$ (1σ) and the algorithms of Crowley and others (2007), resulting in an increase in the $^{206}Pb/^{238}U$ dates of ~0.09 Ma. All common Pb in analyses was attributed to laboratory blank and subtracted based on the measured laboratory Pb isotopic composition and associated uncertainty. U blanks are estimated at 0.013 ± 0.009 pg (1σ).

Weighted mean $^{206}Pb/^{238}U$ dates were calculated from equivalent dates (probability of fit >0.05) using Isoplot 3.0 (Ludwig, 2003). Errors on the weighted mean dates are given as ± x/y/z, where x is the internal error based on analytical uncertainties only, including counting statistics, subtraction of tracer solution, and blank and initial common Pb subtraction, y includes the tracer calibration uncertainty propagated in quadrature, and z includes the ^{238}U decay constant uncertainty propagated in quadrature. Internal errors should be considered when comparing our dates with $^{206}Pb/^{238}U$ dates from other laboratories that used the same EARTHTIME tracer solution or a

tracer solution that was cross-calibrated using EARTHTIME gravimetric standards. Errors including the uncertainty in the tracer calibration should be considered when comparing our dates with those derived from other geochronological methods using the U-Pb decay scheme (for example, laser ablation ICPMS). Errors including uncertainties in the tracer calibration and ^{238}U decay constant (Jaffey and others, 1971) should be considered when comparing our dates with those derived from other decay schemes (for example, $^{40}Ar/^{39}Ar$, ^{187}Re-^{187}Os). Errors for weighted mean dates and dates from individual grains are given at 2σ.

REFERENCES

Bailey, R. H., and Bland, B. H., 2001, Recent developments in the study of the Boston Bay Group *in* West, D. P., and Bailey, R. H., editors, Guidebook for geological field trips in New England: Geological Society of America Annual Meeting, Boston, p. U1-U23.

Barr, S. M., and White, C. E., 1999, Field relations, petrology and structure of Neoproterozoic rocks in the Caledonia Highlands, southern New Brunswick, Canada: Geological Survey of Canada Bulletin 530, 101 p., https://doi.org/10.4095/210354

——— 2004, Geo-compilation of the Caledonia belt of southern New Brunswick: New Brunswick Department of Natural Resources, Minerals, Policy and Planning Division Map Plate 2004-138, scale 1:100,000.

Barr, S. M., Bevier, M. L., White, C. E., and Doig, R., 1994, Magmatic history of the Avalon terrane of southern New Brunswick, Canada, based on U-Pb (zircon) geochronology: The Journal of Geology, v. 102, n. 4, p. 399–409, https://doi.org/10.1086/629682

Barr, S. M., White, C. E., and Macdonald, A. S., 1996, Stratigraphy, tectonic setting, and geological history of Late Precambrian volcanic-sedimentary-plutonic belts in southeastern Cape Breton Island, Nova Scotia: Geological Survey of Canada Bulletin 468, 84 p., https://doi.org/10.4095/208235

Barr, S. M., Davis, D. W., Kamo, S., and White, C. E., 2003, Significance of U-Pb detrital zircon ages in quartzite from peri-Gondwanan terranes, New Brunswick and Nova Scotia, Canada: Precambrian Research, v. 126, n. 1–2, p. 123–145, https://doi.org/10.1016/S0301-9268(03)00192-X

Barr, S. M., Johnson, S. C., Dunning, G. R., van Rooyen, D., White, C. E., and Park, A. F., 2018, U-Pb (zircon) dating in the Caledonia Highlands, southern New Brunswick *in* Keith, E. A., editor, Geoscience Summaries and Other Activities: Information Circular 2018-1 p. 54–59.

Bevier, M. L., and Barr, S. M., 1990, U-Pb age constraints on the stratigraphy and tectonic history of the Avalon terrane, New Brunswick, Canada: The Journal of Geology, v. 98, n. 1, p. 53–63, https://doi.org/10.1086/629374

Bevier, M. L., Barr, S. M., White, C. E., and Macdonald, A. S., 1993, U-Pb geochronologic constraints on the volcanic evolution of the Mira (Avalon) terrane, southeastern Cape Breton Island, Nova Scotia: Canadian Journal of Earth Sciences, v. 30, n. 1, p. 1–10, https://doi.org/10.1139/e93-001

Billings, M. P., 1929, Structural geology of the eastern part of the Boston Basin: American Journal of Science, series 5, v. 18, p. 99–137, https://doi.org/10.2475/ajs.s5-18.104.97

——— 1975, Geology of the North Metropolitan Relief Tunnel, Greater Boston, Massachusetts: Journal of the Boston Society of Civil Engineers, v. 62, p. 115–135.

——— 1976, Geology of the Boston Basin, *in* Lyons, P. C., and Brownlow, A. H., editors, Studies in New England Geology: Geological Society of America Memoirs, v. 146, p. 5–28, https://doi.org/10.1130/MEM146-p5

——— 1982, Ordovician cauldron subsidence of the Blue Hills Complex, eastern Massachusetts: GSA Bulletin, v. 93, n. 9, p. 909–920, https://doi.org/10.1130/0016-7606(1982)93<909:OCSOTB>2.0.CO;2

Billings, M. P., and Tierney, F. L., 1964, Geology of the City Tunnel Extension: Journal of the Boston Society of Civil Engineers, v. 51, p. 111–154.

Chute, N. E., 1966, Geology of the Norwood Quadrangle, Norfolk and Suffolk counties, Massachusetts: United States Geological Survey Bulletin 1163-B, 78 p. Accompanying map at scale 1:24,000.

Clark, T. H., 1923, New fossils from the vicinity of Boston: Proceedings of the Boston Society of Natural History, v. 36, p. 473–485.

Clarke, F. W., 1924, Data of geochemistry: United States Geological Survey Bulletin 770, 841 p., https://doi.org/10.3133/b770

Compston, W., Wright, A. E., and Toghill, P., 2002, Dating the Late Precambrian volcanicity of England and Wales: Journal of the Geological Society, v. 159, n. 3, p. 323–339, https://doi.org/10.1144/0016-764901-010

Condon, D. J., Schoene, B., McLean, N. M., Bowring, S. A., and Parrish, R. R., 2015, Metrology and traceability of U-Pb isotope dilution geochronology (EARTHTIME Tracer Calibration Part I): Geochimica et Cosmochimica Acta, v. 164, p. 464–480, https://doi.org/10.1016/j.gca.2015.05.026

Crosby, W. O., 1888, Geology of the outer islands of Boston Harbor: Proceedings of the Boston Society of Natural History, v. XXIII, p. 450–457.

Crowley, J. L., Schoene, B., and Bowring, S. A., 2007, U-Pb dating of zircon in the Bishop Tuff at the millennial scale: Geology, v. 35, n. 12, p. 1123–1126, https://doi.org/10.1130/G24017A.1

Dillon, P. M., ms, 1994, Geochemistry and petrogenesis of the Late Precambrian plutonic series south of Boston, eastern Massachusetts: Chestnut Hill, Massachusetts, Masters thesis, 150 p.

Dillon, P., Dunning, G., and Hon, R., 1993, Geochemical and geochronological evidence for two distinct

Avalonian magmatic suites, eastern Massachusetts: Geological Society of America Abstracts with Programs, v. 25, n. 2, p. 12.
Dowse, A. M., 1950, New evidence on the Cambrian contact at Hoppin Hill, North Attleboro, Massachusetts: American Journal of Science, v. 248, n. 2, p. 95–99, https://doi.org/10.2475/ajs.248.2.95
Eby, G. N., Wooley, A. R., Din, V., and Platt, G., 1998, Geochemistry and petrogenesis of nepheline syenites: Kasungu—Chipala, Ilomba, and Ulindi nepheline syenite intrusions, North Nyasa Alkaline Province, Malawi: Journal of Petrology, v. 39, n. 8, p. 405–424, https://doi.org/10.1093/petroj/39.8.1405
El Wakeel, S. K., and Riley, J. P., 1961, Chemical and mineralogical studies of deep-sea sediments: Geochimica et Cosmochimica Acta, v. 25, n. 2, p. 110–146, https://doi.org/10.1016/0016-7037(61)90128-4
Garrels, R. M., and Mackenzie, F. T., 1971, Evolution of sedimentary rocks: New York, W.W. Norton & Company, 397 p.
Gerstenberger, H., and Haase, G., 1997, A highly effective emitter substance for mass spectrometric Pb isotope ratio determinations: Chemical Geology, v. 136, n. 3–4, p. 309–312, https://doi.org/10.1016/S0009-2541(96)00033-2
Giles, P. S., and Ruitenberg, A. A., 1977, Stratigraphy, paleogeography, and tectonic setting of the Coldbrook Group in the Caledonia Highlands of southern New Brunswick: Canadian Journal of Earth Sciences, v. 14, n. 6, p. 1263–1275, https://doi.org/10.1139/e77-115
Green, T., Thompson, M., and Davidson, T., 2002, South shore stratigraphy of the Boston Basin: Insights from the Braintree Weymouth Tunnel: Geological Society of America Abstracts with Programs, v. 34, n. 1, p. A15.
Gromet, L. P., Haskin, L. A., Korotev, R. L., and Dymek, R. F., 1984, The "North American shale composite": Its compilation, major and trace elements characteristics: Geochimica et Cosmochimica Acta, v. 48, n. 12, p. 2469–2482, https://doi.org/10.1016/0016-7037(84)90298-9
Hampton, R. L., 2017, The Middlesex Fells Volcanic Complex: A revised tectonic model based on geochronology, geochemistry and field data: American Geophysical Union Fall, abstract #V13D-0410.
Hanson, L., and McFadden, R., 2014, Rocks and landforms of the Lynn Woods and Breakheart Reservations: What they reveal about the local geologic history and what still needs to be cxplored, *in* Thompson, M. D., editor, Guidebook to field trips in southeastern New England (MA-NH-RI): Wellesley, Massachusetts, 106th Meeting of the New England Intercollegiate Geologic Conference, p. C2-1-C2-24.
Haskin, M. A., and Haskin, L. A., 1966, Rare earths in European shales: A redetermination: Science, v. 154, n. 3748, p. 507–509, https://doi.org/10.1126/science.154.3748.507
Heiss, J., Condon, D. J., McLean, N., and Noble, S. R., 2012, $^{238}U/^{235}U$ systematics in terrestrial uranium-bearing minerals: Science, v. 335, n. 6076, p. 1610–1614, https://doi.org/10.1126/science.1215507
Hepburn, J. C., Hon, R., Dunning, G. R., Bailey, R. H., and Galli, K., 1993, The Avalon and Nashoba terranes (eastern margin of the Appalachian orogen in southeastern New England), *in* Cheney, J. T., and Hepburn, J. C., editors, Field Trip Guidebook for the Northeastern United States: Geological Society of America, Annual Meeting, Boston, v. 2, p. ×1–X31.
Hermes, O. D., and Zartman, R. E., 1985, Late Proterozoic and Devonian plutonic terrane within the Avalon zone of Rhode Island: GSA Bulletin, v. 96, n. 2, p. 272–282, https://doi.org/10.1130/0016-7606(1985)96<272:LPADPT>2.0.CO;2
——— 1992, Late Proterozoic and Silurian alkaline plutons within the Southeastern New England Avalon Zone: The Journal of Geology, v. 100, n. 4, p. 477–486, https://doi.org/10.1086/629599
Hibbard, J. P., van Staal, C. R., Rankin, D. W., and Williams, H., 2006, Lithotectonic map of the Appalachian Orogen, Canada-United States of America: Geological Survey of Canada Map 2096A, scale 1:1,500,000, https://doi.org/10.4095/221932
Hirst, D. M., 1962, The geochemistry of modern marine sediments from the Gulf of Paria: I. The relationship between mineralogy and the distribution of the major elements: Geochimica et Cosmochimica Acta, v. 26, n. 2, p. 309–334, https://doi.org/10.1016/0016-7037(62)90017-0
Hiscott, R. N., 1982, Tidal deposits of the Lower Cambrian Random Formation, eastern Newfoundland: Facies and paleoenvironments: Canadian Journal of Earth Sciences, v. 19, n. 10, p. 2028–2042, https://doi.org/10.1139/e82-180
Jaffey, A. H., Flynn, K. F., Glendenin, L. E., Bentley, W. C., and Essling, A. M., 1971, Precision measurements of half-lives and specific activities of ^{235}U and ^{238}U: Physical Review C, v. 4, p. 1889–1906, https://doi.org/10.1103/PhysRevC.4.1889
Kaye, C. A., and Zartman, R. E., 1980, A Late Proterozoic Z to Cambrian age for the stratified rocks of the Boston Basin, Massachusetts, *in* Wones, D. R., editor, The Caledonides in the USA: Blacksburg, Virginia, Virginia Polytechnic Institute and State University Memoir 2, p. 257–261.
Krogh, T. E., 1973, A low contamination method for hydrothermal decomposition of zircon and extraction of U and Pb for isotopic age determinations: Geochimica et Cosmochimica Acta, v. 37, n. 3, p. 485–494, https://doi.org/10.1016/0016-7037(73)90213-5
Krogh, T. E., Strong, D. F., O'Brien, S. J., and Papezik, V. S., 1988, Precise U-Pb zircon dates from the Avalonian terrane in Newfoundland: Canadian Journal of Earth Sciences, v. 25, n. 3, p. 442–453, https://doi.org/10.1139/e88-045
LaForge, L., 1932, Geology of the Boston area, Massachusetts: United States Geological Survey Bulletin 839, 105 p., https://doi.org/10.3133/b839
Landing, E., 1988, Lower Cambrian of eastern Massachusetts: Stratigraphy and small shelly fossils: Journal of Paleontology, v. 62, n. 5, p. 661–695, https://www.jstor.org/stable/1305390
——— 1996, Avalon: Insular continent by the latest Precambrian, *in* Nance, R. D., and Thompson, M. D., editors: Avalonian and related peri-Gondwanan terranes of the circum-North Atlantic: Geological Society of America Special Paper 304, p. 29–63, https://doi.org/10.1130/0-8137-2304-3.29
——— 2004, Precambrian—Cambrian boundary interval deposition and the marginal platform of the Avalon

microcontinent: Journal of Geodynamics, v. 37, n. 3–5, p. 411–435, https://doi.org/10.1016/j.jog.2004.02.014
Lenk, C., Strother, P. K., Kaye, C. A., and Barghoorn, E. S., 1982, Precambrian age of the Boston Basin: New evidence from microfossils: Science, v. 216, n. 4546, p. 619–620, https://doi.org/10.1126/science.216.4546.619
Ludwig, K. R., 2003, User's Manual for Isoplot 3.00: Berkeley, California, Berkeley Geochronology Center, Special Publication, n. 4, 70 p.
Mattinson, J. M., 2005, Zircon U-Pb chemical abrasion ("CA-TIMS") method: Combined annealing and multi-step partial dissolution analysis for improved precision and accuracy of zircon ages: Chemical Geology, v. 220, n. 1–2, p. 47–66, https://doi.org/10.1016/j.chemgeo.2005.03.011
Miller, B. V., Barr, S. M., Fyffe, L. R., and White, C. E., 2000, New U-Pb ages from southern New Brunswick: Preliminary results, *in* Carroll, B. M. W., editor, Current Research 1999: New Brunswick Department of Natural Resources and Energy, Minerals and Energy Division, Mineral Resource Report 2000-4, p. 39–50.
Mills, A., Dunning, G. R., and Langille, A., 2016, New geochronological constraints on the Connecting Point Group, Bonavista Peninsula, Avalon Zone, Newfoundland: Current Research (2016), Newfoundland and Labrador Department of Natural Resources, Geological Survey Report 16-1, p. 153–171.
Moser, A. C., Evans, J. P., Ault, A. K., Janecke, S. U., and Bradbury, K. K., 2017, (U-Th)/He thermochronometry reveals Pleistocene punctuated deformation and synkinematic hematite mineralization in the Mecca Hills, southernmost San Andreas Fault zone: Earth and Planetary Science Letters, v. 476, p. 87–99, https://doi.org/10.1016/j.epsl.2017.07.039
Murphy, J. B., and Nance, R. D., 1989, Model for the evolution of the Avalonian-Cadomian belt: Geology, v. 17, n. 8, p. 735–738, https://doi.org/10.1130/0091-7613(1989)017<0735:MFTEOT>2.3.CO;2
Murphy, J. B., Keppie, J. D., Davis, D., and Krogh T. E., 1997, Regional significance of new U-Pb data for Neoproterozoic igneous units in Avalonian rocks of northern mainland Nova Scotia, Canada: Geological Magazine, v. 134, n. 1, p. 113–120, https://doi.org/10.1017/S0016756897006596
Murphy, J. B., Strachan, R. A., Nance, R. D., Parker, K. D., and Fowler, M. B., 2000, Proto-Avalonia: A 1.2–1.0 Ga tectonothermal event and constraints for the evolution of Rodinia: Geology, v. 28, n. 12, p. 1071–1074, https://doi.org/10.1130/0091-7613(2000)028<1071:PAAGTE>2.3.CO;2
Murray, D. P., Hermes, O. D., and Duham, T. S., 1990, The New Bedford area: A preliminary assessment, *in* Socci, A. D., Skehan, J. W., and Smith, G. W., editors, Geology of the composite Avalon terrane of southern New England: Geological Society of America Special Paper 245, p. 155–169, https://doi.org/10.1130/SPE245-p155
Nance, R. D., and Murphy, J. B., 1996, Basement isotopic signatures and Neoproterozoic paleogeography of Avalonian-Cadomian and related terranes in the circum-North Atlantic, *in* Nance, R. D., and Thompson, M. D., editors, Avalonian and Related Peri-Gondwanan Terranes of the Circum-North Atlantic: Geological Society of America Special Paper 304, p. 333–346, https://doi.org/10.1130/0-8137-2304-3.333
Nance, R. D., Murphy, J. B., and Keppie, J. D., 2002, A Cordilleran model for the evolution of Avalonia: Tectonophysics, v. 352, n. 1–2, p. 11–31, https://doi.org/10.1016/S0040-1951(02)00187-7
Nance, R. D., Murphy, J. B., Strachan, R. A., Keppie, J. D., Gutiérrez-Alonso, G., Fernández-Suárez, J., Quesada, C., Linnemann, U., D'Lemos R., and Pisarevsky, S. A., 2008, Neoproterozoic-early Palaeozoic tectonostratigraphy and palaeogeography of the per-Gondwanan terranes: Amazonian v. West African connections, *in* Ennih, N., and Liégeois, J.-P., editors, The Boundaries of the West African Craton: Geological Society of London Special Publications, v. 297, p. 345–383, https://doi.org/10.1144/SP297.17
Nance, W. B., and Taylor, S. R., 1976, Rare earth element patterns and crustal evolution—I. Australian post-Archean sedimentary rocks: Geochimica et Cosmochimica Acta, v. 40, n. 12, p. 1539–1551, https://doi.org/10.1016/0016-7037(76)90093-4
Noble, S. R., Condon, D. J., Carney, J. N., Wilby, P. R., Pharaoh, T. C., and Ford, T. D., 2015, U-Pb geochronology and global context of the Charnian Supergroup, UK: Constraints on the age of key Ediacaran fossil assemblages: GSA Bulletin, v. 127, n. 1–2, p. 250–265, https://doi.org/10.1130/B31013.1
O'Brien, S. J., O'Brien, B. H., Dunning, G. R., and Tucker, R. D., 1996, Late Neoproterozoic Avalonian and related per-Gondwanan rocks of the Newfoundland Appalachians, *in* Nance, R. D., and Thompson, M. D., editors, Avalonian and related peri-Gondwanan terranes of the circum-North Atlantic: Geological Society of America Special Paper 304, p. 9–28, https://doi.org/10.1130/0-8137-2304-3.9
Plank, T., and Langmuir, C. H., 1998, The chemical composition of subducting sediment and its consequences for the crust and mantle: Chemical Geology, v. 145, n. 3–4, p. 325–394, https://doi.org/10.1016/S0009-2541(97)00150-2
Plank, T., and Ludden, J. N., 1992, Geochemistry of sediments in the Argo Abyssal Plain at site 765: A continental margin reference section for sediment recycling in subduction zones, *in* Gradstein, F. M., and Ludden, J. N., editors, Proceedings of the Ocean Drilling Program: Scientific Results, v. 123, p. 167–189, https://doi.org/10.2973/odp.proc.sr.123.158.1992
Potter, J., Longstaffe, R. J., Barr, S. M., Thompson, M. D., and White, C. E., Altering Avalonia: Oxygen isotopes and terrane distinction in the Appalachian peri-Gondwanan realm: Canadian Journal of Earth Sciences, v. 45, n. 7, p. 815–825, https://doi.org/10.1139/E08-024
Pe-Piper, G., and Piper, D. J. W., 2002, A synopsis of the geology of the Cobequid Highlands, Nova Scotia: Atlantic Geology, v. 38, n. 2–3, p. 145–160, https://doi.org/10.4138/1259
Pu, J. P., Bowring, S. A., Ramezani, J., Myrow, P., Raub, T. D., Landing, E., Mills, A., Hodgin, E., and Macdonald, F. A., 2016, Dodging snowballs: Geochronology of the Gaskiers glaciation and the first

appearance of the Ediacaran biota: Geology, v. 44, n. 11, p. 955–958, https://doi.org/10.1130/G38284.1
Rahm, D. A., 1962, Geology of the Main Drainage Tunnel: Journal of the Boston Society of Civil Engineers, v. 49, p. 319–368.
Rast, N., O'Brien, B. H., and Wardle, R. J., 1976, Relationships between Precambrian and Lower Palaeozoic rocks of the 'Avalon Platform' in New Brunswick, the northeast Appalachians and the British Isles: Tectonophysics, v. 30, n. 3–4, p. 325–338, https://doi.org/10.1016/0040-1951(76)90192-X
Reynolds, P. H., Barr, S. M., and White, C. E., 2009, Provenance of detrital muscovite in Cambrian Avalonia of Maritime Canada: $^{40}Ar/^{39}Ar$ ages and chemical compositions: Canadian Journal of Earth Sciences, v. 46, n. 3, p. 169–180, https://doi.org/10.1139/E09-013
Richardson, S. M., 1977, Geology of the Dorchester Tunnel, Boston, Massachusetts: Journal of the Boston Society of Civil Engineers, v. 63, p. 247–269.
Rodgers, J., 1967, Chronology of tectonic movements in the Appalachian region of eastern North America: American Journal of Science, v. 265, n. 5, p. 408–427, https://doi.org/10.2475/ajs.265.5.408
——— 1972, Latest Precambrian (post-Grenville) rocks of the Appalachian region: American Journal of Science, v. 272, n. 6, p. 507–520, https://doi.org/10.2475/ajs.272.6.507
Schmitz, M. D., and Schoene, B., 2007, Derivation of isotope ratios, errors and error correlations for U-Pb geochronology using ^{205}Pb-^{235}U-(^{233}U)-spiked isotope dilution thermal ionization mass spectrometric data: Geochemistry, Geophysics, Geosystems, v. 8, n. 8, Q08006, https://doi.org/10.1029/2006GC001492
Shaler, N. S., 1869, On the relations of the rocks in the vicinity of Boston: Proceedings of the Boston Society of Natural History, v. XIII, p. 172–177.
Skehan, J. W., Murray, D. P., Palmer, A. R., Smith, A. T., and Belt, E. S., 1978, Significance of fossiliferous Middle Cambrian rocks of Rhode Island to the history of the Avalonian microcontinent: Geology, v. 6, n. 11, p. 694–698, https://doi.org/10.1130/0091-7613(1978)6<694:SOFMCR>2.0.CO;2
Sláma, J., Košler., J, Condon, D. J., Crowley, J. L., Gerdes, A., Hanchar, J. M., Horstwood, M. S. A., Morris, G. A., Nasdala, L., Norberg, N., Schaltegger, U., Schoene, B., Tubrett, M. N., and Whitehouse, M. J., 2008, Plešovice zircon—A new natural reference material for U–Pb and Hf isotopic microanalysis: Chemical Geology, v. 249, n. 1–2, p. 1–35, https://doi.org/10.1016/j.chemgeo.2007.11.005
Spengler, S. R., and Garcia, M. O., 1988, Geochemistry of the Hawi lavas, Kohala Volcano, Hawaii: Contributions to Mineralogy and Petrology, v. 99, p. 90–104, https://doi.org/10.1007/BF00399369
Spotila, J. A., Niemi, N., Brady, R., House, M., Buscher, J., and Oskin, M., 2007, Long-term continental deformation associated with transpressive plate motion: The San Andreas Fault: Geology, v. 35, n. 11, p. 967–970, https://doi.org/10.1130/G23816A.1
Sun, S. S., and McDonough, W. F., 1989, Chemical and isotopic systematics of oceanic basalts: Implications for mantle composition and processes, *in* Saunders, A. D., and Norry, M. J., editors, Magmatism in the Ocean Basins: Geological Society, London Special Publications, v. 42, p. 313–345, https://doi.org/10.1144/GSL.SP.1989.042.01.19
Tanoli, S. K., and Pickerill, R. K., 1988, Lithostratigraphy of the Cambrian-Lower Ordovician Saint John Group, southern New Brunswick: Canadian Journal of Earth Sciences, v. 25, n. 5, p. 669–690, https://doi.org/10.1139/e88-064
Taylor, S. R., and McLennan, S. M., 1985, The continental crust: Its composition and evolution: Oxford, England, Blackwell Scientific Publications, 312 p.
Taylor, S. R., McLennan, S. M., and McCulloch, M. T., 1983, Geochemistry of loess, continental crustal composition and crustal model ages: Geochimica et Cosmochimica Acta, v. 47, n. 11, p. 1897–1905, https://doi.org/10.1016/0016-7037(83)90206-5
Thompson, M. D., and Bowring, S. A., 2000, Age of the Squantum "Tillite," Boston Basin, Massachusetts: U-Pb zircon constraints on terminal Neoproterozoic glaciation: American Journal of Science, v. 300, n. 8, p. 630–655, https://doi.org/10.2475/ajs.300.8.630
Thompson, M. D., Hermes, O. D., Bowring, S. A., Isachsen, C. E., Besancon, J. R., and Kelly, K. L., 1996, Tectonostratigraphic implications of Late Proterozoic U-Pb zircon ages in the Avalon Zone of southeastern New England, *in* Nance, R. D., and Thompson, M. D., editors, Avalonian and related peri-Gondwanan terranes of the circum-North Atlantic: Geological Society of America Special Paper 304, p. 179–191, https://doi.org/10.1130/0-8137-2304-3.179
Thompson, M. D., Grunow, A. M., and Ramezani, J., 2007, Late Neoproterozoic paleogeography of the Southeastern New England Avalon Zone: Insights from U-Pb geochronology and paleomagnetism: Geological Society of America Bulletin, v. 119, n. 5–6, p. 681–696, https://doi.org/10.1130/B26014.1
Thompson, M. D., Ramezani, J., Barr, S. M., and Hermes, O. D., 2010, High-precision U-Pb zircon dates for Ediacaran granitoid rocks in SE New England: Revised magmatic chronology and correlation with other Avalonian terranes, *in* Tollo, R. P., Bartholomew, M. J., Hibbard, J. P., and Karabinos, P. M., editors, From Rodinia to Pangea: The lithotectonic record of the Appalachian Region: Geological Society of America Memoir 206, p. 231–250, https://doi.org/10.1130/2010.1206(11)
Thompson, M. D., Barr, S. M., and Grunow, A. M., 2012, Avalonian perspectives on Neoproterozoic paleogeography: Evidence from Sm-Nd isotopic geochemistry and detrital zircon geochronology in SE New England, USA: GSA Bulletin, v. 124, n. 3–4, p. 517–531, https://doi.org/10.1130/B30529.1
Thompson, M. D., Ramezani, J., and Crowley, J. L., 2014, U-Pb zircon geochronology of Roxbury Conglomerate, Boston Basin, Massachusetts: Tectono-stratigraphic implications for Avalonia in and beyond SE New England: American Journal of Science, v. 314, n. 6, p. 1009–1040, https://doi.org/10.2475/06.2014.02
Thompson, P. J., Kopera, J., Ross, M., Bailey, R., and Thompson, M., 2014, Bedrock geology of Boston Harbor: Cambridge Argillite and associated diabase sills and debris flows, *in* Thompson, M. D., editor, Guidebook to field trips in southeastern New England (MA-NH-RI): Wellesley, Massachusetts, 106th Meeting of the New England Intercollegiate Geologic Conference, p. C1-1-C1-32.

Underwood, M. B., and Pickering, K. T., 1996, Clay-mineral provenance, sediment dispersal patterns, and mudrock diagenesis in the Nankai accretionary prism, southwest Japan: Clays and Clay Mineralogy, v. 44, n. 3, p. 339–356, https://doi.org/10.1346/CCMN.1996.0440304

van Staal, C. R., and Barr, S. M., 2012, Lithospheric architecture and tectonic evolution in the Canadian Appalachians and associated Atlantic margin, *in* Percival, J. A., Cook, F. A., and Clowes, R. M., editors, Tectonic styles in Canada: the LITHOPROBE perspective: Geological Association of Canada Special Paper 49, p. 41–95.

Volckmann, R. P., 1977, Bedrock geologic map of the Holliston and Medfield quadrangles. Middlesex, Norfolk, and Worcester counties, Massachusetts: United States Geological Survey Miscellaneous Investigations Series I-1053, scale 1:48,000.

Walsh, G. J., Aleinikoff, J. N., and Dorais, M. J., 2009, Tectonic history of the Avalon and Nashoba terranes along the western flank of the Milford antiform, Massachusetts: Geological Society of America Abstracts with programs, v. 41, n, 3, p. 98.

Watson, E. B., Wark, D. A., and Thomas, J. B., 2006, Crystallization thermometers for zircon and rutile: Contributions to Mineralogy and Petrology, v. 151, p. 413–433, https://doi.org/10.1007/s00410-006-0068-5

Weaver, C. E., 1989, Clays, muds, and shales: Amsterdam, Elsevier Science Publishers, Developments in Sedimentology, v. 44, 819 p.

White, C. E., MacHattie, T. G., Neyedley, K., and Barr, S. M., 2019, The Cobequid Highlands, Nova Scotia, Canada: Extending the Avalonian geological record back to the early Neoproterozoic: Geological Society of America Abstracts with Programs, v. 51, n. 1, ISSN 0016-7592, https://doi.org/10.1130/abs/2019NE-328156

White, C. E., Barr, S. M., van Rooyen, D., and Crowley, J. L., 2020, The Mount Ephraim Block, Cobequid Highlands, Nova Scotia: A significant *ca.* 750-735 Ma magmatic arc event in Avalonia: Geological Society of America Abstracts with Programs, v. 52, n. 2, ISSN 0016-7592, https://doi.org/10.1130/abs/2020SE-344176

Williams, H., 1978, Tectonic lithofacies map of the Appalachian orogen: Memorial University of Newfoundland Map No. 1, scale 1:1,000,000.

Wilner, A. P., Barr, S. M., Gerdes, A., Massonne, H.-J., and White, C. E., 2013, Origin and evolution of Avalonia: Evidence from U-Pb and Lu-Hf isotopes in zircon from the Mira terrane, Canada, and the Stavelot—Venn Massif, Belgium: Journal of the Geological Society, London, v. 170, n. 5, p. 769–784, https://doi.org/10.1144/jgs2012-152

Wintsch, R. P., Kvale, C. M., and Kisch, H. J., 1991, Open-system, constant-volume development of slaty cleavage, and strain-induced replacement reactions in the Martinsburg Formation, Lehigh Gap, Pennsylvania: GSA Bulletin, v. 103, n. 7, p. 916–927, https://doi.org/10.1130/0016-7606(1991)103<0916:OSCVDO>2.3.CO;2

Zartman, R. E., and Naylor, R. S., 1984, Structural implications of some radiometric ages of igneous rocks in southeastern New England: GSA Bulletin, v. 95, n. 5, p. 522–539, https://doi.org/10.1130/0016-7606(1984)95<522:SIOSRA>2.0.CO;2

Zartman, R. E., Hermes, O. D., and Pease Jr., M. H., 1988, Zircon crystallization ages and subsequent isotopic disturbance events, in gneissic rocks of eastern Connecticut and western Rhode Island: American Journal of Science, v. 288, n. 4, p. 376–402, https://doi.org/10.2475/ajs.288.4.376

Zen, E-an, 1983, Bedrock geologic map of Massachusetts: United States Geological Survey, 3 sheets, scale 1:250,000.